Volume II.G

Midwestern Regional Carbon Sequestration Partnership (MRCSP) Phase III (Development Phase)

Assessment of Borehole Gravity (Density) Monitoring for CO_2 Injection into the Dover 33 Reef

Prepared by:

Battelle
505 King Avenue
Columbus, Ohio 43201

Principal Investigator: Dr. Neeraj Gupta

Authors: Matthew Place, Alain Bonneville, Andrew Black, and Neeraj Gupta

Submitted to:

The U.S. Department of Energy, National Energy Technology Laboratory
Program Manager: Andrea McNemar

DOE MRCSP Project #DE-FC26-05NT42589

September 2020

Notice

This report was prepared by Battelle as an account of work sponsored by an agency of the United States Government and other project sponsors, including Core Energy, LLC and The Ohio Development Services Agency. Neither the United States Government, nor any agency thereof, nor any of their employees, nor Battelle and other cosponsors, makes any warranty, express or implied, or assumes any liability or responsibility for the accuracy, completeness, or usefulness of any information, apparatus, product, or process disclosed, or represents that its use would not infringe privately owned rights. Reference herein to any specific commercial product, process, or service by trade name, trademark, manufacturer, or otherwise does not necessarily constitute or imply its endorsement, recommendations, or favoring by the United States Government or any agency thereof. The views and the opinions of authors expressed herein do not necessarily state or reflect those of the United States Government or any agency thereof.

Battelle does not engage in research for advertising, sales promotion, or endorsement of our clients' interests including raising investment capital or recommending investments decisions, or other publicity purposes, or for any use in litigation.

Battelle endeavors at all times to produce work of the highest quality, consistent with our contract commitments. However, because of the research and/or experimental nature of this work the client undertakes the sole responsibility for the consequence of any use or misuse of, or inability to use, any information, apparatus, process or result obtained from Battelle, and Battelle, its employees, officers, or Trustees have no legal liability for the accuracy, adequacy, or efficacy thereof.

Acknowledgements

Sponsorships - This report is part of a series of reports prepared under the Midwestern Regional Carbon Sequestration Partnership (MRCSP) Phase III (Development Phase). These reports summarize and detail the findings of the work conducted under the Phase III project. The primary funding for the MRCSP program is from the US Department of Energy's National Energy Technology Laboratory (NETL) under DOE project number DE-FC26-05NT42589 with Ms. Andrea McNemar as the DOE project manager. The past DOE project managers for MRCSP include Dawn Deel, Lynn Brickett, and Traci Rodosta. Many others in the DOE leadership supported, encouraged, and enabled the MRCSP work including but not limited to Kanwal Mahajan, John Litynski, Darin Damiani, and Sean Plasynski.

The Michigan Basin large-scale test received significant in-kind cost share from Core Energy, LLC, who also provided essential access to the field test site and related data. This contribution by Core Energy CEO Robert Mannes, VP Operations Rick Pardini, and Allan Modroo, VP Exploration, and the entire Core Energy staff is gratefully acknowledged. MRCSP work in Ohio has been supported by the Ohio Coal Development Office in the Ohio Development Services Agency under various grants (CDO D-10-7, CDO-D-13-22, CDO-D-D-13-24, and CDO-D-15-08) with Mr. Greg Payne as the OCDO project manager. Finally, several industry sponsors and numerous technical team members from State Geological Surveys, universities, and field service providers have supported MRCSP through cash and in-kind contributions over the years as listed in the individual reports.

Program Leadership – During the MRCSP Phase III project period, several Battelle staff and external collaborators contributed to the successful completion of the program through their efforts in field work, geological data analysis and interpretation, and/or reporting. The primary project managers over the MRCSP performance period have included Rebecca Wessinger, Neeraj Gupta, Jared Walker, Rod Osborne, Darrell Paul, David Ball. Additional project management support has been provided by Andrew Burchwell, Christa Duffy, Caitlin McNeil, and Jacqueline Gerst over the years.

Principal Investigator: Neeraj Gupta (614-424-3820/ gupta@battelle.org)

Report Authors and Principal Technical Contributors – Matthew Place, Alain Bonneville (PNNL), Andrew Black (Tellus Gravity)

Other Technical Contributors – Lydia Cumming, Benjamin Grove, Mark Kelley, and Samin Raziperchikolaee, Glenn Larsen, Ethan Mann, Jennifer Hare

Table of Contents

List of Tables

List of Figures

List of Equations

Page

Acronyms and Abbreviations

BHG	Borehole Gravity
CCL	Casing Collar Locator
CO_2-EOR	Carbon-dioxide enhanced oil recovery
DOE	Department of Energy
GR	Natural Gamma
MEMS	Electric Mechanical Systems
MRCSP	Midwestern Regional Carbon Sequestration Partnership
MT	Metric tons
NETL	National Energy Technology Laboratory
OOIP	Original oil in place
OWC	Oil Water Contact
PNNL	Pacific Northwest National Laboratory
TVD	True Vertical Depth
WLD	Wireline Depth

1.0 Introduction and Background

1.1 Introduction

MRCSP was established to assess the technical potential, economic viability, and public acceptability of carbon sequestration within its region. It was established by the Department of Energy (DOE) National Energy Technology Laboratory (NETL) as part of its overall strategy to 1) develop technologies that will support industries' ability to predict CO_2 storage capacity in geologic formations to within ±30%; 2) develop technologies to demonstrate that 99 percent of injected CO_2 remains in the target injection zones; and 3) contribute technical expertise and lessons learned for development of best practices. Objectives for the project include assessing new technologies for tracking CO_2, brine, and oil movements underground; and monitoring options in a closed reservoir with oil, residual oil zone, and water zones. The borehole gravity (BHG) surveys were completed to specifically investigate the ability of this technology to monitor the flow and storage zones of the injected CO_2 during the injection and production stages.

Between 2013 and 2016, Core Energy (Battelle) injected 264,586 metric tons of CO_2 into a nearly depleted oil and gas reef known as Dover 33. Between July 2016 and July 2018, 136,271 tons of CO_2 were produced from this reef, leaving 128,315 tons of CO_2 remaining in the reef. There was also a relatively small amount of oil produced in that time. The 2018 reservoir pressure was approximately midway between the 2013 and 2016 reservoir pressures.

Three BHG surveys were performed (2013, 2016, and 2018) to monitor the changes in gravity/density as a result of the injection and withdraw of CO_2 into and from the reef. The gravity/density changes were then modeled to determine the flow and storage zones of the injected CO_2 in the reef.

This report presents the results of BHG surveys conducted in the Lawnichak-Myskier (L-M) 1-33 well in the Dover 33 reef by Tellus Gravity and Micro-g LaCoste in 2013, 2016, and 2018. A comparison of the data from the three surveys was performed to determine the feasibility of BHG to detect and monitor the location of the injected CO_2 (i.e., CO_2 plume) in the reef over time. In addition, modeling was performed to compare the field data with the modeled data.

Applying time-lapse BHG monitoring to a carbon sequestration site consists of determining temporal gravity anomalies related to the injection of CO_2, and exclusively associated to the redistribution of the fluids in the pore space (Figure 1-1). Gravity measurements must be performed exactly at the same locations during each survey event.

The initial two BHG surveys were performed in 2013 and 2016 by Micro-g LaCoste and the 2018 survey was performed by Tellus Gravity LLC, both under agreements with Battelle. Tellus Gravity LLC is a company formed with former Micro-g LaCoste employees that split off from Micro-g LaCoste in early 2018. Tellus personnel were also involved in the 2013 and 2016 BHG surveys in planning, survey operations, data processing and modeling. The two reports presenting the results for these three surveys were used as a basis of the present study (Black & Mann, 2018; Hare et al.; 2017).

All three surveys used the Gravilog borehole gravity tool manufactured by Scintrex, Ltd (Nind et al., 2013). The 2013 survey used Gravilog™ S/N 9 and the 2016 and 2018 surveys both used Gravilog S/N 16. It has a specified sensitivity of 5 microGals and is operable in boreholes deviated from vertical to 60 degrees from vertical. Gravity measurements were taken at 39 downhole stations observed between the depths 650 ft (198 m) and 5,538 ft. (1,688 m) using a typical method for BHG surveys (Robbins, 1989; Beyer, 1983). Survey data is provided in Appendix A.

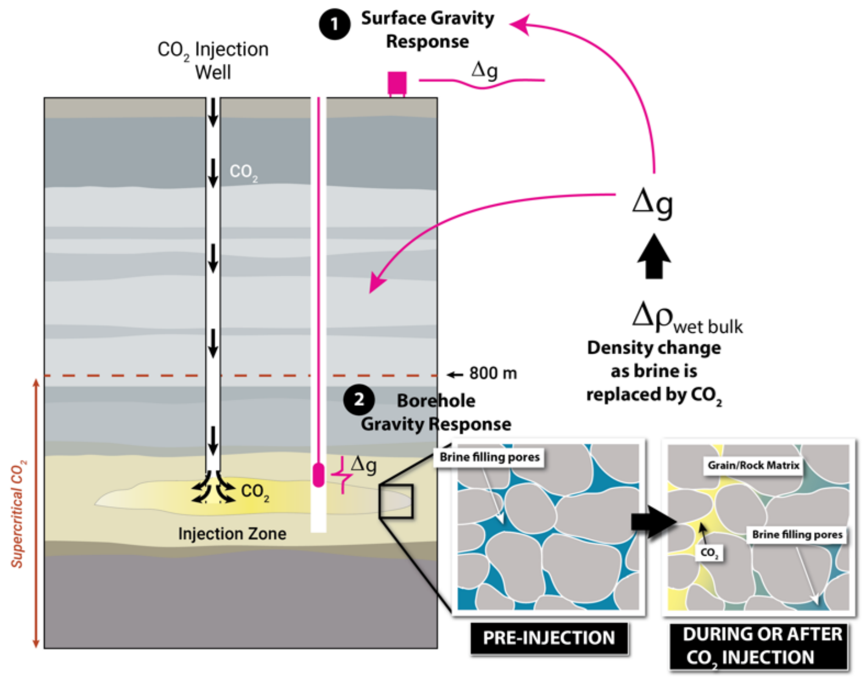

Figure 1-1. Principle of time-lapse gravity monitoring. The injection of CO_2 in the reservoir leads to the gradual replacement of original pore filling fluids by CO_2. This mass redistribution can be detected using surface gravity surveys (1), and borehole gravity survey (2) (from Appriou & Bonneville, 2020).

1.2 Background to Dover 33 Reef Geology

The Dover 33 reef is an isolated reef structure in the northern Niagaran pinnacle reef trend that is approximately 270 ft (82 m) thick at a depth of about 5,400 ft (1,650 m) (top of reef). The reservoir is in the end stages of recovery, having undergone primary production and several steps of secondary oil recovery with CO_2 injection. Table 1-1 presents the lithology/stratigraphy through the Dover 33 reef complex.

Table 1-1. Stratigraphy through the Dover 33 reef complex.

Formation Name	Depth to Top of Formation (ft MD)
Salina B Salt	4,875 (1,486 m)
A2 Carbonate	5,205 (1,586 m)
A2 Evaporite	5,281 (1,610 m)
A1 Carbonate	5,308 (1,618 m)
Brown Niagaran	5,373 (1,638 m)
Gray Niagaran	5,645 (1,721 m)
Oil/Water Contact	5,471 (1,667 m)

In the Dover 33 reef, the reservoir includes both the Brown Niagaran and A-1 Carbonate Formations, and wireline log data from 13 wells around the reef were analyzed to develop the detailed geologic structure of the reef. The interpretations of the log data were used to divide the reef into zones based on reservoir potential (Haagsma et al., 2020). Figure 1-2 illustrates the divisions of the interpreted lithofacies in map view. Four lithofacies were defined: 1) Windward (purple) with high flow potential, 2) Reef Core (green) which includes the reef core facies with moderate to high flow potential, 3) Leeward (blue) which includes the leeward facies with low to moderate flow potential and 4) includes the flanks and off-reef Brown Niagaran Formation with no flow potential. The reef core was subdivided into the Reef Apron and Bioherm based on small-scale geologic data, both of which are composed of mixed limestone and dolomite with moderate to high porosity. The A-1 Carbonate Formation showed moderate porosity with occasional salt plugs. Moderate porosity/storage potential was observed in the distal reef apron and rubble where there was vugular dolomite.

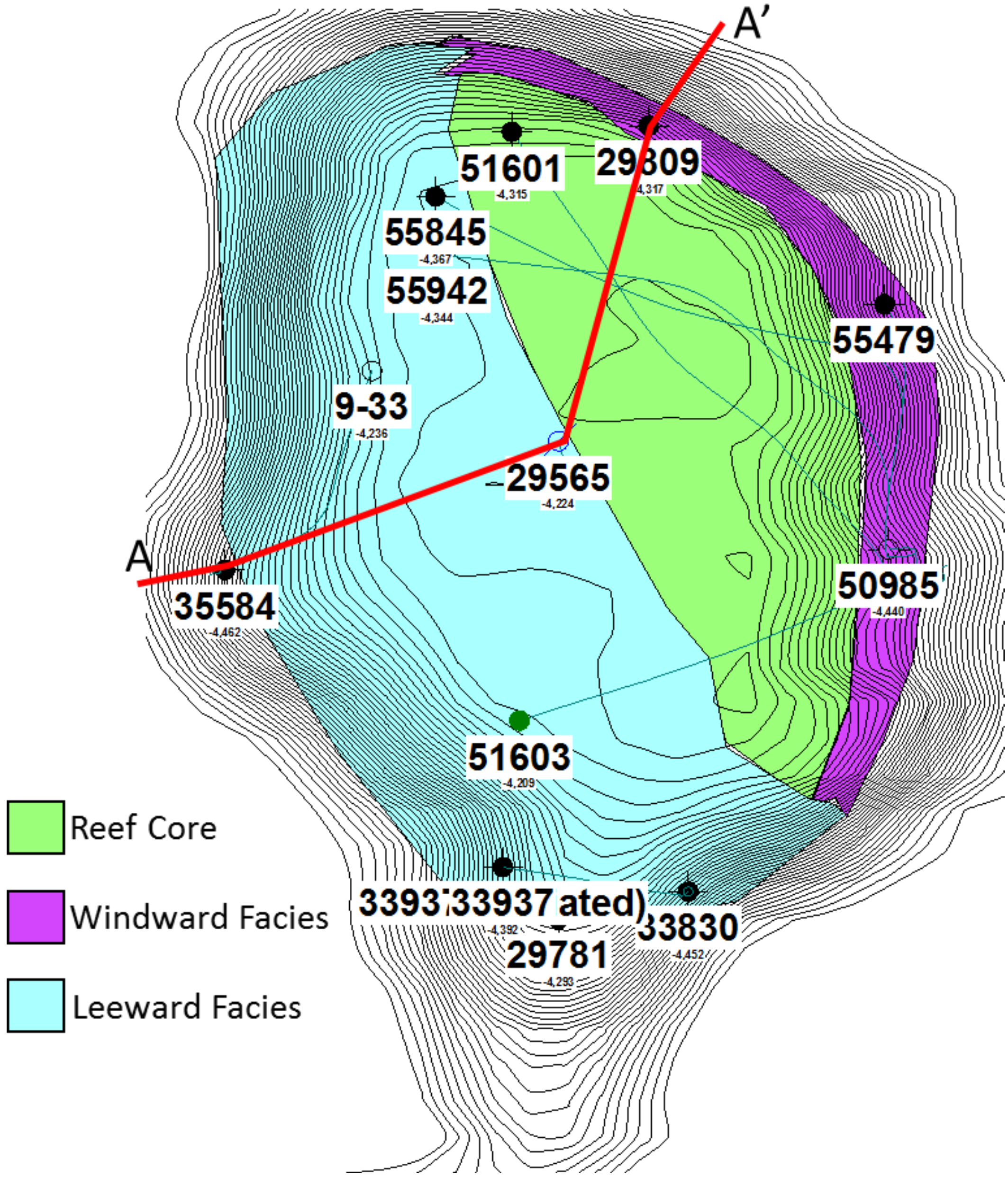

Figure 1-2. Plan view of the depositional model of the Dover 33 reef field showing the subdivision into windward (purple), reef core (green), and leeward (blue) facies (Haagsma et al., 2020).

An interpreted cross section was constructed across the reef (A-A’) to illustrate the changes in lithology and the locations of the lithofacies. Cross section A-A’ (Figure 1-3) illustrates the thicker salts and carbonates off reef and the thinning of the A-1 and A-2 Carbonate Formations on the crest of the reef. Internally, the leeward facies are to the southwest, the reef core is central, and the windward facies are to the northeast.

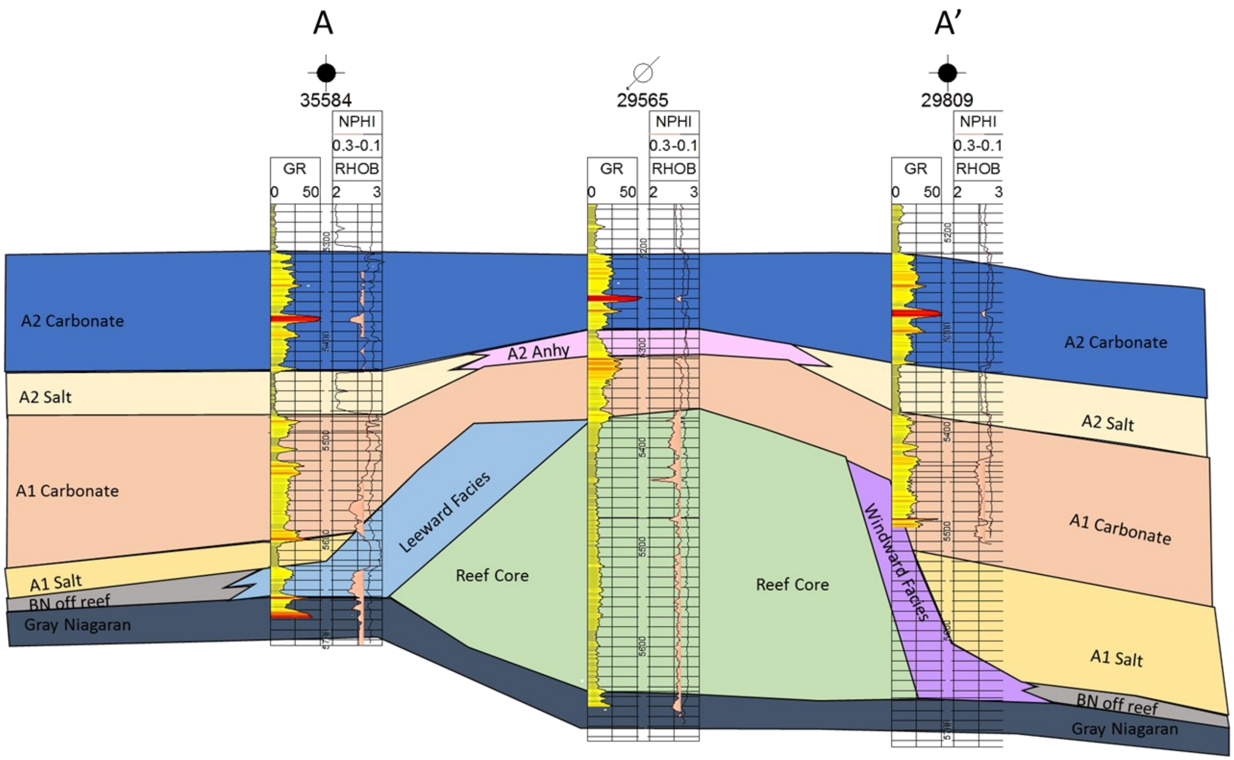

Figure 1-3. Cross section A-A’ across the northern reef pod in the Dover 33 reef field showing changes in lithology and lithofacies from the southwest to the northeast (Haagsma et al., 2020).

1.3 Background to Borehole Gravity Technology

Measuring gravity is a potentially useful method for monitoring of changing fluid distributions within a reservoir. The method is a passive measurement of the existing gravity field and it bridges the radius of investigation gap between the near-borehole examination by well logging tools and the larger volumes examined by many of the seismic methods. In a time-lapse mode, the method is responsive only to temporal density distribution changes, such as those associated with CO_2 injection and production.

However, the accuracy requirements for time-lapse gravity surveys can seem daunting since the signals are on the order of tens of microGals. To be relevant, the gravity tool must measure differences in gravity over time to within a few microGals. Because the normal vertical gravity gradient within a well is approximately 29 microGal/foot (see Section 2, Table 2-2), the tool must be placed at the same measurement locations during each of the time lapse surveys (ideally to within 0.1 foot).

BHG measurements are collected over discrete intervals in the borehole by stopping the BHG meter at preselected observation depths, often referred to as stations. The most powerful use of the BHG meter is as a density logger. The vertical gradient of gravity (z), $\Delta g/\Delta z$, is determined for the interval of interest by measuring the gravity difference, Δg, and the vertical distance between two consecutive stations, Δz. The assumption made to calculate apparent density ρ_a is based on an earth model composed of infinitely extended horizontal slabs (Figure 1-4).

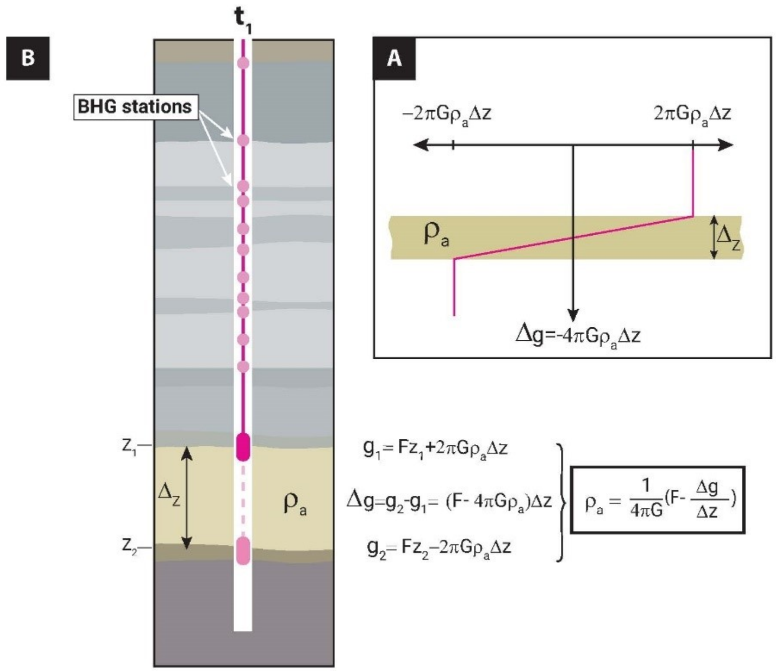

Figure 1-4. Cross section of the gravitational model for an infinitely extended horizontal slab (a) and its application in a borehole for the determination of the density (b) at a specific time (t1) (from Appriou & Bonneville, 2020).

The density of each slab is related to the gravity gradient measured in that interval. The free-air gravity gradient, which is affected by the shape of the earth and the height of the station, also contributes to gravity acceleration and must be taken into consideration. The measured gravity acceleration is, therefore, a function of both the free-air effect and the slab density effect, which leads to the fundamental equation for determining BHG (Beyer, 1983; LaFehr, 1983).

$$\Delta g = (F - 4\pi\rho_a G)\Delta z$$

Equation 1-1

where F is the free-air gradient at the borehole location (0.3086 mGal/m) and G is the Newtonian gravitational constant (G=6.631024 m3 kg-1 s-2). Using this fundamental equation, the average density ρ_a between two BHG stations may then be written as

$$\rho_a = \frac{F - \Delta g/\Delta z}{4\pi G}$$

Equation 1-2

Regarding the radius of investigation into the formation, ρ_a is an averaged value over a volume about five times the vertical spacing between two adjacent stations (Robbins, 1989). The volume that can be investigated by a borehole gravimeter provides a unique advantage of the method compared to volumes sampled by traditional logging tools that typically are limited to the volume within centimeters of the borehole, or within the borehole itself from core data analysis. This also means that borehole gravity densities are not affected by the casing and borehole rugosity (Robbins, 1989). Because of the large investigation volume at the Michigan field site, the formation density measured within a Niagaran reef structure is often lower than the open hole gamma density log due to the presence of lower density halite flanking the reefs.

Using survey practical English and metric units, Equation 1-2 reduces to:

$$\rho_a = \; 3.68237 - 0.005247\, sin^2\phi - 39.1200\frac{\Delta g}{\Delta z}$$

Equation 1-3

where Δg is in milliGal (1 mGal = 10-5 m/s2), Δz in feet, and ρ_a in g/cm3.

Gravilog tools have a specified tool repeatability of 5 microGal (1microGal = 10-8 m/s2) or better when measured in laboratory testing. “Repeatability” refers to the standard deviation of multiple gravity measurements after applying all necessary corrections. For survey statistics, repeatability is reported at a single station (the ‘station repeatability’ or sigma), or as an average repeatability of all stations for a complete well survey, the survey repeatability. For surveys, an additional uncertainty is produced by the variation of the tool depths at each station resulting in station repeatabilities that are slightly larger than the tool repeatability (i.e., the internal precision of the tool – repeatability of measurements for the exact same conditions).

The station accuracy for a single station is calculated by dividing the repeatability at that station by the square root of N, where N is the number of repeat readings at that station. When ‘station accuracy’ is referenced, it specifies the standard deviation of the final estimated gravity value at that station.

The estimated apparent density error from borehole gravity, $\in (\rho_a)$, depends on the estimated station accuracy and the vertical station interval. Larger measurement intervals produce smaller BHG density errors. A good approximation of the conventional apparent density error, ε(ρa), in g/cm3 is given by:

$$\in (\rho_a) = \; 39.12\, \frac{\in (g)}{dz}$$

Equation 1-4

where ε(g) is the station gravity error in milliGal and dz is the station spacing in feet.

Note, that apparent density estimates based on Equation 1-2 and Equation 1-3 must be corrected for well deviation in significantly deviated wells since the equations assume vertical depths.

Time-lapse surface gravity methods are well developed and have been used quite successfully for reservoir monitoring over the past few decades (e.g., Van Gelderen et al., 1999; Hare et al., 1999; Brady et al., 2006; Ahmad Zamri et al., 2009, Eiken, et al. 2008). The time-lapse borehole gravity method is less established, but analogous methods exist to obtain reliable, repeatable positions and gravity measurements in a borehole (e.g., Van Popta et al., 1990; Krahenbuhl and Li, 2012; Krahenbuhl et al., 2012; Hare and Black, 2015; Rim and Li, 2015 and Black et al., 2016). A summary for each of the papers is presented below.

Van Popta et al., 1990. This paper described the results of a field application of borehole gravimetry to measure secondary gas saturations in a fractured limestone reservoir. The survey relied on the deep-reading capability and insensitivity to near-wellbore effects, to obtain measurements that could not be collected with conventional cased-hole logging methods. Borehole-fluid pressure data, recorded together with the gravity data, proved useful in ensuring that the density data had the necessary high accuracy. This paper additionally presented modelling results that indicated the potential usefulness of time-lapse borehole gravity data for monitoring flood fronts remote from a borehole.

Krahenbuhl and Li, 2012. This study utilized complex model construction and robust inversion methods to show that time-lapse gravity surveys may contribute to improved production efficiency and reservoir management. The authors used published data from the Jotun Field in the Norwegian North Sea, which is a well-studied site that has demonstrated the successful application of time-lapse seismic techniques and has been reconstructed for 4D gravity.

Krahenbuhl et al., 2012. This paper provides a study on the benefit of jointly inverting surface and borehole gravity data for reservoir monitoring. In particular, the authors show that time-lapse measurements in horizontal monitoring wells can provide additional information about fluid movement over surface data alone. The paper discusses the primary advantage of such monitoring wells lies in the option to preferentially orient them with the geometry of a production or sequestration field. In addition, well heights can be designed to maximize the signal strength in consideration of instrument accuracy, while balancing data sensitivity to the lateral extent of the reservoir to be monitored. This study demonstrated these benefits using a realistic representation of a complex CO_2-EOR site and the joint interpretation of surface and borehole data with highly constrained inversion.

Hare and Black, 2015. This study examined the use of surface and borehole gravity surveys for monitoring reservoir density changes in light of current instrumentation precision, survey logistical constraints, and type of reservoir operation. The authors reviewed the applicable state-of-the-art gravity instruments, and the capabilities and limitations of microgravity for time-lapse monitoring are discussed in the context of several large reservoir monitoring projects. Finally, the authors outline important lessons learned from these projects for future use of the time-lapse gravity method for reservoir monitoring.

Rim and Li, 2015. In this paper, the authors presented a time-lapse inversion method for determining the front of injected "CO_2" using borehole gravity measurements. The authors assume that the horizontal extent of the fluid can be represented by a polygon with known but variable thickness and density contrast due to fluid substitution. The evolution of the fluid front is represented as a 4d function of the spatial position and time from the beginning of injection. The authors show that the inversion can be carried out either independently at discrete time points or as a single inversion simultaneously over all time points. They demonstrate that performing a single inversion simultaneously over all time points is the superior technique because it is more stable and offers improved capability in detecting break-through events at later times.

Black et al., 2016. The authors provide baseline data for a borehole gravity survey performed in the Aquistore PTRC ESTEVAN OBS 5-6-2-8 CO_2 sequestration observation well adjacent to the Boundary Dam coal fired power plant near Estevan, Saskatchewan. The data from the gravity survey are compared to ɣɣ density data from wireline logs performed prior to CO_2 injection. The comparison of the data show both positive and negative variances between the two logs that may be attributed to well installation processes, differences in geologic conditions away from the borehole, the injection of the CO_2, and/or errors in the logging tools.

A major distinction exists between single-event gravity surveys, where the goal is to recover absolute earth densities and density distributions, and time-lapse gravity surveys, where density changes over time are measured.

Time-lapse density changes are calculated directly from the time-lapse gravity changes using the following modified BHG equation:

$$\Delta_{(t2-t1)}\,\rho_a = -39.1200\left[\left(\Delta_{(t2-t1)}g_{z2} - \Delta_{(t2-t1)}g_{z1}\right)/(z_2 - z_1)\right]$$

Equation 1-5

where

$\Delta_{(t2-t1)}\,\rho_a$ is the 4D interval density in g/cm^3 between stations at depths z_2 and z_1,

$\Delta_{(t2-t1)}g_{z2}$ is the change in observed gravity at the depth z_2 station between time t_2 and t_1,

$\Delta_{(t2-t1)}g_{z1}$ is the change in observed gravity at the depth z1 station between time t2 and t1, and
$(z_2 - z_1)$ is the spacing between the two stations in feet.

The largest sources of spatial gravity variations are the free-air effect, latitude effect, and regional and local geology, including terrain, lithology, and structural variations. These time-static sources of gravity variation are cancelled by time-differencing survey data from different times. The remaining time-lapse, or 4D, signal is representative of temporal changes in formation densities (such as those due to CO_2 or other fluid injections or redistributions). The time-variable density changes of interest for monitoring a CO_2 plume are often two orders of magnitude smaller than lithologic variations, hence the need for careful tool calibration, station positioning, and microGal-precision measurements for time-lapse surveys.

A combination of natural gamma logs and high-resolution casing collar locator (CCL) logs can be used for repositioning stations to within a few centimeters or less. Repeated passes through multiple stations are used in the borehole as the basis for computation of a least-squares drift correction. Corrections are applied for temperature, pressure, tilt, earth tides, and ocean loading. Differential depth corrections are applied for station reoccupation differences. Downhole gyro surveys enable 3D calculations of the borehole gravity station locations relative to surface stations. The borehole measurements can be tied to surface measurements at the wellhead or other reference points.

The time-lapse gravity errors may be estimated by adding the single-event station gravity errors in quadrature and the time-lapse density errors may be estimated from a modified version of Equation 1-3.

1.4 Gravilog™ System

All three BHG surveys used the Gravilog™ borehole gravity tool manufactured by Scintrex, Ltd. The 2013 survey used Gravilog™ S/N 9 and the 2016 and 2018 surveys both used Gravilog™ S/N 16 (see Figure 1-5 for specifications for the Gravilog™ system). Scintrex originally developed the Gravilog™ tool for mining and geotechnical applications. The gravity sensor is based on the fused-quartz technology, which has proven to be rugged and accurate in land exploration gravity meters (most recently the CG-5 and CG-6 Autograv systems). This basic sensor technology has been miniaturized and equipped with self-leveling capabilities for use for borehole gravity surveys. The associated electronics modules have been packaged to fit into a narrow-diameter borehole sonde. Each Gravilog™ tool has been designed to log inside standard mining diamond drilling NQ (57 mm I.D.) drill rods or oil field 2 7/8-inch diameter tubing. It has a specified sensitivity of 5 microGals and is operable in boreholes deviated from vertical to 60 degrees from vertical.

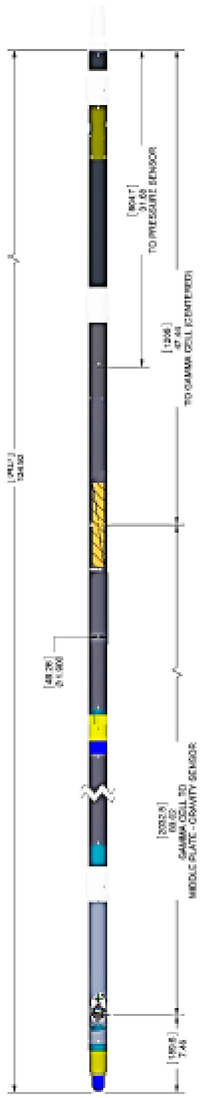

Table A1. Gravilog Tool System Specifications

Temperature Range:	0° C to + 80° C (32° F to 176° F)
Maximum Pressure:	27,500 kPa (3700 PSI)
Inclination:	Vertial (0°) to 60° from vertical
Outside Diameter:	48.26 mm (1.9")
Length:	4 m (13.725')
Weight:	38.6 kg (85 lb)
Repeatability:	5 µGal (<50 nms^{-2})
Conductors:	Operates on 4 to 7 conductor cables

The tool incorporates a wall lock arm and natural gamma detector, well temperature, well pressure and inclination sensors.

Tool consists of several modules listed from the top module:

- Clamp module
- Pressure/Gamma module
- Electronics module
- Gravilog module
- Shock mount

The distances between the sensors are used to correct the output readings to the gravity sensor depth as described in the BlueGrav Data Acquisition Software manual.

Table A2. Gravilog Tool Distnace Between Sensors

Gravity sensor to tool bottom:	18.96 cm
Gravity sensor to Gamma detector:	203.25 cm
Gravity sensor to pressure sensor:	243.28 cm
Gravity sensor to top clamp module:	323.75 cm
Gravity sensor to top MSI tool head:	338.20 cm
Gravity sensor to top MSI cable head spring:	368.04 cm

Figure 1-5. Diagram of Scintrex gravilog tools used in the BHG surveys

Improvements were made by the manufacturer to the Gravilog™ system between the 2013 and 2016 surveys and again between the 2016 and 2018 surveys. The major improvements between 2013 and 2016 included the replacement of bubble levels with more stable micro-electromechanical systems (MEMS) tilt sensors, improvements to electronics related to robustness and environmental stability. Incremental modifications to the internal gravity sensor also improved the robustness and decreased the propensity to tare.

For 2018, the change to the tool was the addition of the high-resolution casing collar locator (CCL) module. This involved the replacement of the previous gamma detection module with a gamma/CCL module manufactured by Spartek. This module allows the tool to be re-located within metal tubing or casing to an accuracy of about 1 inch.

2.0 Survey Methods

2.1 Dover 33 and Lawnichak-Myszkier 1-33 Well

The BHG survey was conducted in the Lawnichak-Myszkier (L-M) 1-33 in the Dover 33 reef. The Dover 33 reef is in northern Michigan, Otsego County, near the town of Gaylord. The L-M 1-33 well is a vertical well located near the center of the reef and serves as the sole CO_2-injection well for the reef (Figure 2-1). Figure 2-1 also displays nearby wells with wireline logging data available. The L-M 1-33 has a 5-1/2-inch-diameter casing from surface to 5,665 ft (Figure 2-2) and is completed across the A-1 Carbonate and Brown Niagaran Formations (Figure 2-3). The MRCSP injection of CO_2 (2013-2016) and the production of fluids (2016-2018) occurred in the perforated interval between the depths of 5,309 ft and 5,460 ft. During BHG surveys, the tubing string was extended from the surface (wellhead) to with a few feet of the bottom of the well to allow for passage of BHG tool.

Figure 2-1. Dover 33 location map indicating the location of the L-M 1-33 well and surrounding wells with geophysical log data availability.

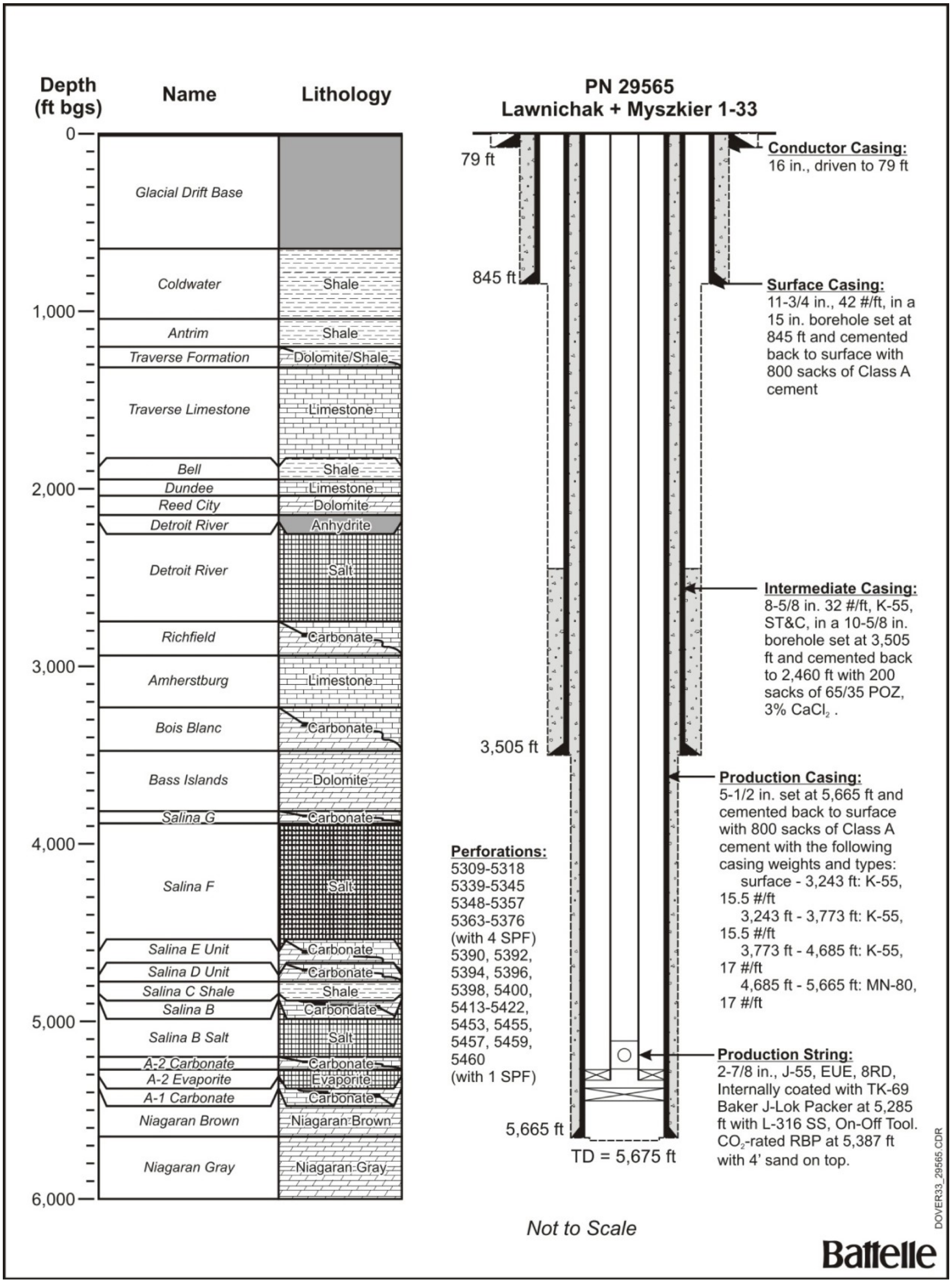

Figure 2-2. Well completion diagram for the Lawnichak-Myszkier 1-33 well.

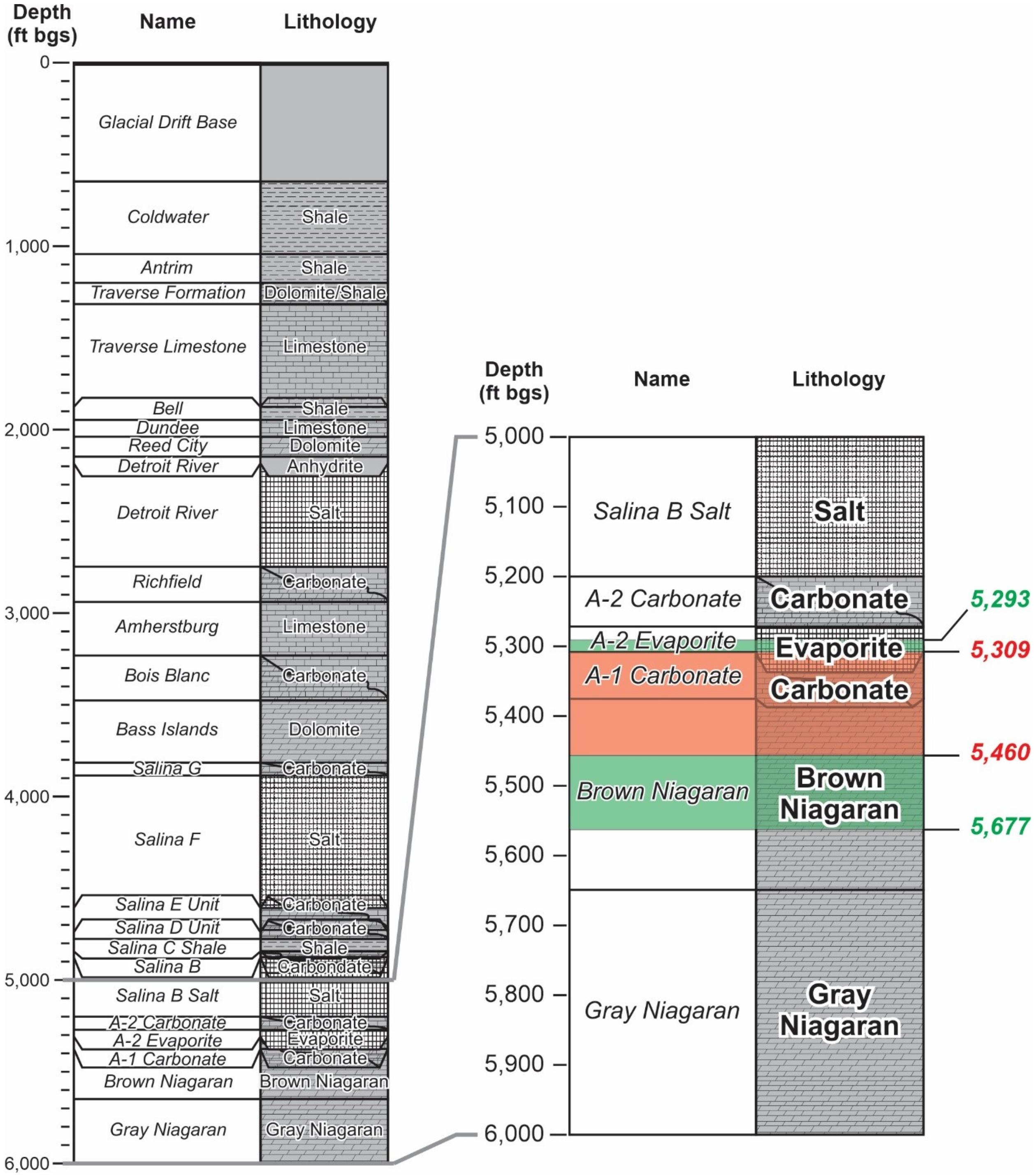

Figure 2-3. Lithologic section and spatial extension of the reef geologic model (in green) and the perforated zone (in orange).

For the 2013 baseline BHG survey, the reservoir pressure was approximately 800 psi with residual gaseous CO_2 remaining in the reef from the initial CO_2 EOR activities (1995-2012). For the 2016 survey, the reservoir pressure was approximately 3,500 psi with a CO_2 density of 880 kg/m3 (7.3 lb/gal) resulting from the injection of CO_2 into the reef. During the last survey in July 2018, the reservoir pressure was approximately 1,200 psi and a CO_2 density of 290 kg/m3 (2.3 lb/gal). Figure 2-4 summarizes the changes in fluid mass between the BHG surveys and provides an indication of changes expected between the three gravity surveys. Between the 2013 and 2016 surveys, 264,586 metric tons of CO_2 were injected into the reef while 6 metric tons of oil and 16 metric tons of brine were removed from the reef, resulting in a net change of 264,564 metric tons. The reef went into a production phase between the 2016 and 2018 surveys and 136,271, 4,243, and 2,542 metric tons of CO_2, oil, and brine, respectively were removed from the reef, reducing the overall bulk density in the reef. Figure 2-5 displays images of the BHG survey field operations performed in 2018.

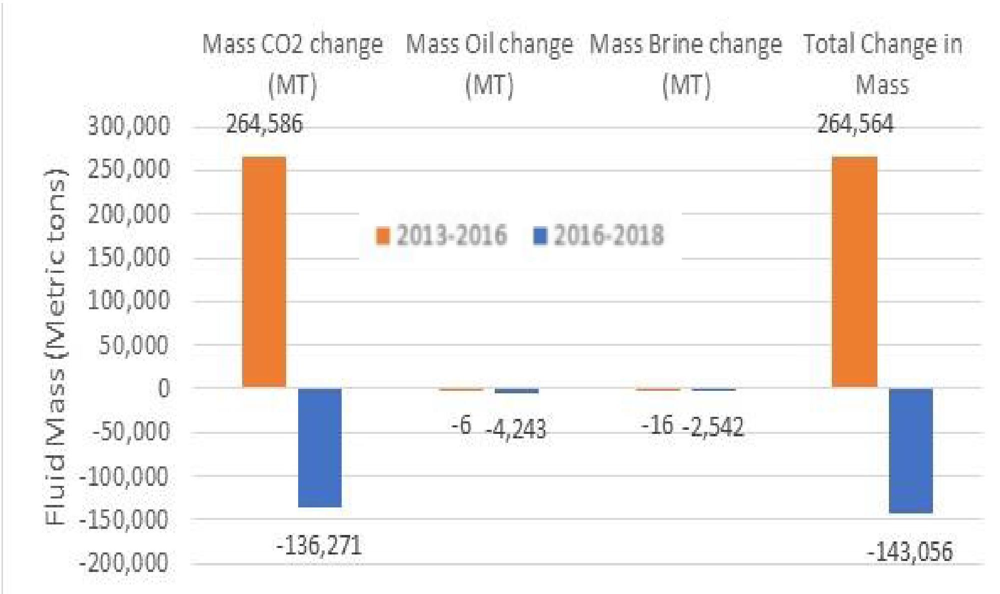

Figure 2-4. Changes in reservoir fluid mass between 2013-2016 (orange) and 2016-2018 (blue).

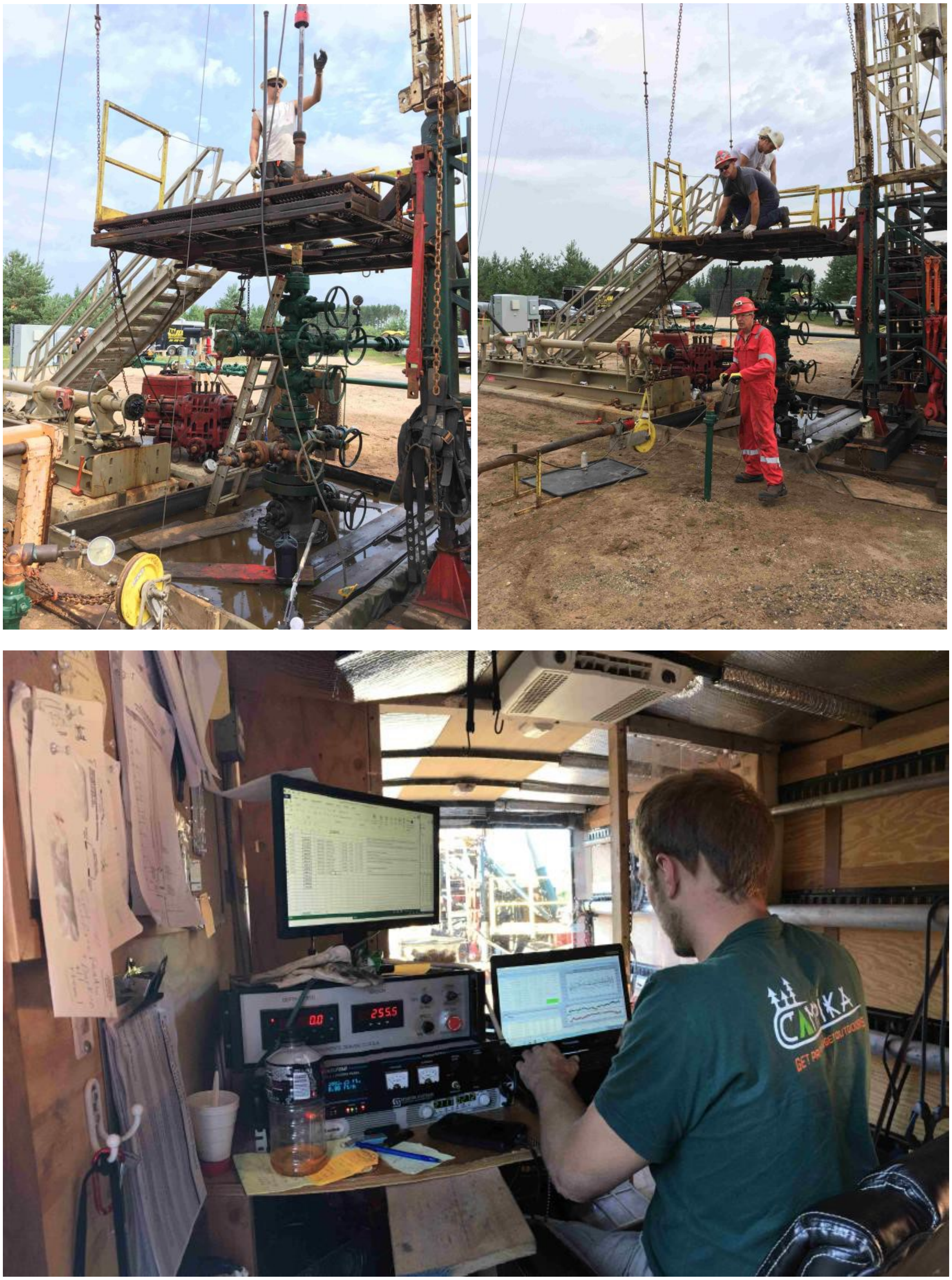

Figure 2-5. Dover 33 2018 borehole gravity survey photos. Upper right: Dover 33 wellhead. Upper left: Gravilog™ rig up with tool in riser pipe. Lower: Operating Gravilog™ uphole instrumentation.

2.2 Survey Approach

The surveys performed in 2013, 2016, and 2018 all included the same station depths and number of logging passes or sweeps per zone. The surveys were divided into three zones plus three near-surface stations for a total of approximately 40 stations, depending on the survey. An extra logging pass (sweep) through deep reef zone (Zone 1) was performed during the 2018 survey as QC data processing after the first four sweeps indicated a unique drift pattern was negatively impacting data accuracy. While performing this fifth pass, it was found that the tidal corrections used during Passes 1 through 4 had been calculated for the default file settings location of a Colorado test well. The tidal corrections were corrected in post processing and no additional readings were made related to this issue.

Table 2-1 provides the division of the zones and depths used during the three BHG surveys in the L-M 1-33 well. A combination of surface wireline odometer, natural gamma (GR), and CCL measurements were used to control measurement depths for the 2018 Dover 33 (L-M 1-33) BHG survey. In 2013 and 2016, the CCL tool was not available and only the odometer and GR were used to determine the depth.

Table 2-1. Zones, station spacings, depths, and numbers of sweeps during the BHG surveys.

Zone	Station Spacing	Depth (MD)	Number of Sweeps
Zone 1	20 to 40 ft	5,176-5,540 ft	5
Zone 2	120 to 280 ft	3,253-5,176 ft	3
Zone 3	190 to 380 ft	660-3253 ft	3
Near Surface Zone	3 Stations	10, 34, and 240 ft	1

In 2013, the Gravilog™ GR was depth correlated with a pre-existing open hole GR log within the Zone 1 reef section and a cased hole GR log above the reef.

In 2016, the Gravilog™ GR was used to establish a Global Reference Log from just above TD to near surface. This Global Reference GR Log was then correlated with the 2013 GR logs recorded during the 2013 Gravilog™ survey. A similar approach was used in 2018 to establish the 2018 Global GR Log and obtain a listing of the 2013 measurement station positions referred to the 2018 Global GR Log depths. After checking the correlation of the 2018 Global GR Log through the Zone 1 reef section, it was necessary to shift the entire 2018 Global GR Log by 0.72 feet. The resulting log is called the 2018_Shift_Global_GR.las log. The corresponding CCL log using the same depth reference is the 2018_Shift_Global_CCL.las log. This CCL log was the primary depth reference used throughout the 2018 survey to correlate the tool depths for the multiple sweeps in real time due to its superior depth resolution compared to the gamma log. This increases the certainty in 2018 of positioning multiple readings at the same target depth. The accuracy of reoccupying the same depth as occupied in 2013 and 2016 relies on the gamma log correlations between the different years.

2.3 Nominal Station Depth Corrections

The vertical gradient of gravity in a well is dependent on the formation density, but averages about 1 microGal/cm for a rock density of 2.5 g/cm3. The ability to return to the same depth for time-lapse comparison of gravity is critical.

Although every effort is made to re-occupy the same depth stations with each logging run, the depth control will inevitably have small errors, due to cable stretch, slippage of the manually controlled winch, and slight under or over shooting of depth by the operator. These depth errors were evaluated by comparing the CCL logs acquired when moving the tool with the 2018_Shift_Global_CCL.las log.

The depths for all occupations at a given station (repeat sweeps) were averaged together to give the Nominal Depth for that station. This will inevitably be slightly offset from the 2013 Nominal Station Depths referred to as the Target Depths. In 2018, a further correction was made for the difference between the Nominal and Target Station Depths.

Table 2-2 displays approximate vertical gradients in a homogeneous half-space in a well with the lithologies observed in the L-M 1-33 well.

Table 2-2. Density estimates and vertical gravity gradients for the rock types observed in the L-M 1-33 well.

Rock Type	Density (g/cm^3)	Vertical Gradient (μGal/ft)	Vertical Gradient (μGal/m)
Halite	2.165	39	128
Limestone	2.71	25	82
Dolomite	2.86	21	69
Anhydrite	2.96	18	59

Note that at stations where the rock density varies significantly from the average (2.55 g/cm3), the station depth corrections will not totally mitigate this source of error. In halite there are an additional 10 microGal/ft and in anhydrite there are an additional 11 microGal/ft in the opposite direction. Since there is no existing gamma density log for the well, these additional gravity gradient corrections have not been made to the data.

The depth corrections for 2013, 2016, and 2018 surveys were calculated using an average gravity gradient for the well of 29 microGal per meter corresponding to a bulk density of 2.55 g/cm3 calculated between the deepest and shallowest gravity measurements (See Table 2-3).

Table 2-3. Corrected depths for the 2013, 2016, and 2018 surveys.

Survey Zone	Station StnID	TVDSS 2013 (ft, msl)	TVD 2013 (ft)	MD2013* Zwld2013 (ft)	MD2016** Zwld2016 (ft)	MD2018# Zwld2018 (ft)	MDClient# # Z-SNP (ft)	Stn Spacing dZtvd2013 (ft)
	37			23.56		23.56		
	36			230.02	240.50	230.02		
3	35	486.02	650.01	650.04	660.50	661.64	651.40	190.01
3	34	305.03	840.02	840.06	850.60	851.76	842.00	335.78
3	33	-31.74	1175.80	1176.07	1186.60	1187.87	1179.20	302.81
3	32	-335.54	1478.61	1479.08	1489.60	1490.58	1483.20	325.91
3	31	-662.45	1804.52	1805.09	1815.80	1815.79	1810.30	306.98
3	30	-971.43	2111.50	2112.08	2122.60	2122.00	2119.30	245.98
3	29	-1217.41	2357.48	2358.08	2368.61	2367.38	2365.10	203.99
3	28	-1420.41	2561.47	2562.08	2572.10	2571.18	2568.80	383.99
3	27	-1804.39	2945.46	2946.08	2954.60	2952.88	2952.30	299.96
2	26	-2103.38	3245.42	3246.06	3253.40	3251.06	3251.40	185.99
2	25	-2289.37	3431.41	3432.05	3438.70	3436.95	3437.20	123.97
2	24	-2413.36	3555.38	3556.04	3562.40	3560.44	3561.00	141.99
2	23	-2554.35	3697.37	3698.03	3704.30	3702.03	3702.80	181.99
2	22	-2736.34	3879.36	3880.03	3886.00	3883.53	3884.60	218.00
2	21	-2954.34	4097.36	4098.03	4102.50	4100.83	4102.40	283.98
2	20	-3238.30	4381.34	4382.04	4385.90	4384.34	4386.00	125.95
2	19	-3363.26	4507.29	4508.04	4511.60	4510.34	4511.90	144.95
2	18	-3508.21	4652.23	4653.03	4656.10	4654.63	4656.70	192.95
2	17	-3701.12	4845.19	4846.06	4848.70	4846.96	4849.50	167.68
2	16	-3868.84	5012.86	5014.03	5016.30	5014.83	5017.30	161.67
1	15	-4028.52	5174.53	5176.02	5176.60	5176.02	5177.80	40.92
1	14	-4069.44	5215.45	5217.02	5217.17	5217.02	5218.80	29.95
1	13	-4099.38	5245.39	5247.02	5246.92	5247.02	5248.70	28.92
1	12	-4128.33	5274.32	5276.00	5275.93	5276.00	5277.70	29.93
1	11	-4158.27	5304.25	5305.99	5306.00	5305.99	5307.60	14.00
1	10	-4172.24	5318.24	5320.01	5320.00	5320.01	5321.60	29.92
1	9	-4202.18	5348.16	5349.99	5350.00	5349.99	5351.60	19.97
1	8	-4222.14	5368.13	5370.00	5370.00	5370.00	5371.60	19.97
1	7	-4242.10	5388.10	5390.01	5390.00	5390.01	5391.50	19.97
1	6	-4262.06	5408.07	5410.02	5410.00	5410.02	5411.50	19.98
1	5	-4282.03	5428.06	5430.04	5430.00	5430.04	5431.50	19.91
1	4	-4301.99	5447.97	5449.99	5450.00	5449.99	5451.50	29.98
1	3	-4331.94	5477.95	5480.03	5480.00	5480.03	5481.50	29.96
1	2	-4361.89	5507.91	5510.03	5510.00	5510.00	5511.40	29.95
1	1	-4391.85	5537.86	5540.03	5540.00	5540.00	5541.40	-

**GR log files: Gaylord-z1-s1-010413-GR.las, Gaylord-z2-s2-010613-GR.las, and Gaylord-z3-s2-010613-Grsplit.las*

***GR log file: Dover33_20160910_GlobalGamma.las*

GR log file: gl16_2018-07-16_33-1-Shift_Global_gamma.las

2.4 Processing Flow

Tellus Gravity used a MatlabTM-based program for post-processing the borehole gravity data. This program reads the raw 1-Hz field-recorded data, allows manual editing of raw observations, computes and applies various gravity corrections including a least-squares fit for drift. The basic processing steps of the data processing are outlined in Table 2-4.

Table 2-4. Post-processing procedure for borehole gravity data

Process Activity	Detail
QC and edit raw 1 Hz time-series gravity occupations (despike, remove initial meter recovery interval (if needed), or exclude entire bad (noisy) occupations),	• No spikes were observed in the 2018 Gravilog™ survey data. All recoveries were positive except for a very few and all were of low amplitude except for two readings that the meter beam stuck at and then was freed. • Raw 1 Hz occupation noise ranged from 6 to 18 microGals
Average individual 1 Hz measurements over the occupation period (typically 300 to 600 seconds),	• Occupation periods averaged approximately five minutes per station and range from four to 20 minutes.
Merge multiple data files from different, sweeps/sections of the well.	• Four or five sweeps were acquired and used in Zone 1; 3 sweeps each in Zones 2 and 3.
Compute observation true vertical depth (TVD) from recorded wireline depth (WLD) using downhole survey control,	• The L-M 1-33 well is nearly vertical, but TVDs computed in 2016 were from interpolated downhole survey data provided in 2013 (file: downholesurvey.xls dated 6/14/2013).
Compute observation latitude, longitude (from 3D downhole survey control, if applicable)	• No corrections were applied for the variation of gravity with latitude as this has no influence on time-lapse gravity differences.
Compute the station depth corrections (corrects each occupation to the mean (nominal) depth of all occupations of a given station).	• A reading depth correction was computed based on the average depth (nominal) for each station. • A station depth correction density of 2.55 g/cm3 was used for this correction (best fit for entire well, and the same as that used for 2013 survey processing). • Re-compute gravity depth corrections to put occupations (and stations) on depth for target depths from previous surveys.
Pre-apply corrections to each station occupation for:	• Sensor tilt • Gravitational tide – recomputed for Zone 1 sweeps 1 through 4 • Ocean loading - recomputed for Zone 1 sweeps 1 through 4 • BHGM temperature • Station depth
Evaluate residuals for outliers, tares (discrete offsets in gravity readings) and breaks (offsets and drift rate changes).	• During the 2018 survey, it was decided to use a single tare after the third reading of Zone 3 of about -54 microGals • A single occupation was excluded in the processing from Zone 1 at 5306’ in sweep 5 during 2018.
Iterative re-computation/evaluation of least squares drift and gravity residuals with occupation edits, tares, and breaks	
Evaluate validity of additional least-squares fit for temperature parameters.	• F-test indicated additional temperature corrections were not statistically significant and were not applied in the processing.

Process Activity	Detail
Average occupations for final station depth, gravity and error estimates.	
Compute BHGM conventional and inversion interval densities and error estimates.	

The data generated during the 2013 survey were processed in 2013 and then reprocessed in 2016 with upgrades to the LRS-BHGM software, and the gravity residuals (station repeat residuals after corrections) are fair with an overall station accuracy of 5.8 microGal and an overall repeatability of 10.8 mGal. A total of two occupations were skipped in the 2013 reprocessing. Two small, approximately 30 mGal, tares were observed in the 2013 BHG data. The 2016 data were processed including measurements over the entire depth range of the well, from ground surface to 5,500 ft. A total of eight single occupations were skipped in the processing, and no breaks or tares were indicated in the data to achieve these results. For the 2016 survey, the gravity residuals are excellent with an overall station accuracy of 2.8 microGal and a survey repeatability of 5.2 microGal. The gravity residuals for the 2018 survey are excellent with an overall repeatability of 5.4 microGal and a station accuracy of 2.6 microGal.

The Bouguer gravity, g_B, is the raw recorded gravity, gr, corrected for the Free Air Gradient and the vertical gravity gradient due to a background earth density, referred to as the Bouguer density, ρ_B. The Bouguer gravity (g_B) is assigned a value of zero at a convenient Bouguer gravity reference depth, zr (Equation 2-1). A depth of 5,320 feet 2013 WLD within the A1 Carbonate Unit was chosen as the reference depth (zr) as this allows for the best comparison between the three sets of data within the reservoir. The Bouguer density used is 2.690 g/cm3, corresponding to the average BHG density measured in the 2013 survey through the Brown Niagaran unit. Note that Bouguer gravity increasing with depth corresponds to lower BHG density values.

$$g_B = g_r + (z - z_r)\left(F - 4\pi G\rho_B\right)$$

Equation 2-1

The standard equation for calculating interval density from BHG data is given by Equation 2-2. Interval densities computed in this manner are referred to by Tellus Gravity as Conventional Densities, which is a synonymous term to slab, interval, and BHGM density.

$$\rho_{BHG} = \frac{1}{4\pi G}\left(F - \frac{\Delta g}{\Delta z}\right)$$

Equation 2-2

The LRS-BHGM program also computes Inversion Densities. This method allows stable calculation of interval densities over much closer station spacings than are feasible using the conventional method. In the presence of noisy data and small station spacing, the inversion densities tend to be smoother, more conservative estimates than conventional densities. The damped least-squares techniques used in the inversion stabilizes the density calculations in several ways:

1. The gravity readings from all stations are used jointly to invert for densities, making use of the inherent redundancy of borehole gravity data
2. The observed gravity data, which contain some amount of error, are not fit exactly, but only to within a tolerance determined by the noise level of the data (regularized inversion)

3. Given the inherent non-uniqueness of gravity inversion, multiple density models may reproduce the observed gravity within a specified tolerance. The inversion calculates the one model out of the set of possible models that has the smallest deviation (in a least-squares sense) from a constant density.

A more detailed summary of the borehole gravity inversion method can be found in MacQueen (2007).

3.0 Gravity Survey Results

The data generated from the 2013, 2016, and 2018 BHG surveys are presented in this section. To best display the time lapse differences, Figure 3-1 shows the BHG density and Bouguer gravity values within the reservoir interval. When these data are viewed for the entire well, the small variations over time are not visible due to the horizontal vs vertical scale of the plot. In addition, the effects of the CO_2 injection would be limited to the reservoir zone. Data from the 2013, 2016, and 2018 BHG surveys are presented in 0.

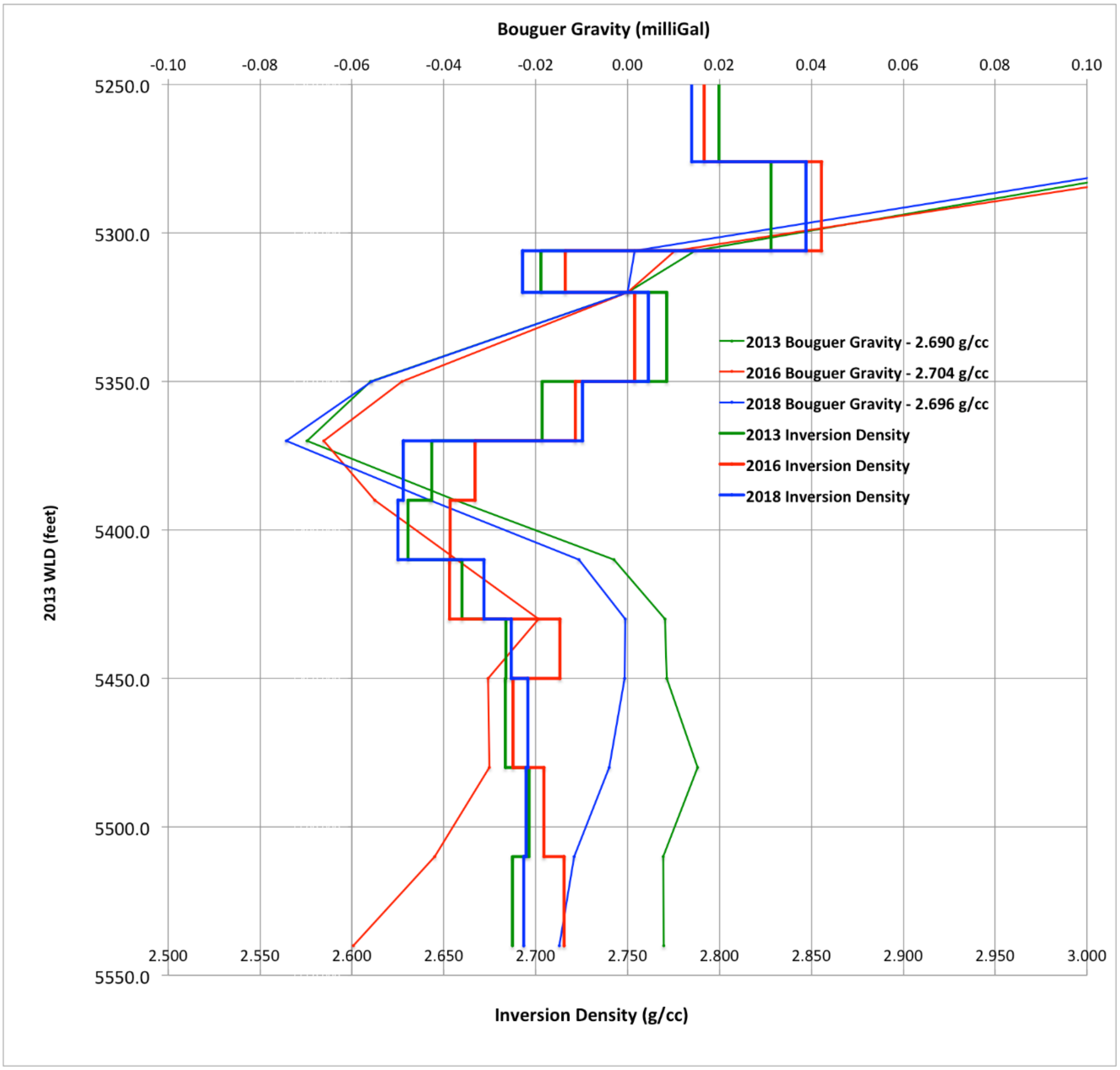

Figure 3-1. Density and Bouguer Gravity measurements within the reservoir zone made during the 2013, 2016, and 2018 BHG Surveys.

3.1 Time-Lapse Gravity Analysis

3.1.1 Time-Lapse Density Differences

A major distinction exists between single-time-epoch gravity surveys and the time-lapse surveys. In single-time surveys, the goal is to recover BHG densities, and time-lapse surveys, where BHG density changes over time are determined. In time-lapse surveys, gross problems due to terrain, regional, and local geology adjacent to the surveyed well cancel out. The time-lapse gravity signals, i.e., the gravity signal differences between the 2013, 2016, and 2018 surveys are only related to changes in subsurface density distribution. In this project, the changes that were investigated are those due to the injection of CO_2 into the reservoir.

Table 3-1 and Table 3-2 show the BHG densities measured during the three surveys performed in 2013, 2016, and 2018. Above the reservoir (Figure 3-2), the BHG density values between the three surveys are relatively comparable and all show zones with low density geologic formations (i.e., the Detroit River Salt between 2,300 and 2,700 feet, the Salina F Salt between 3,900 and 4,700 feet, and the Salina B Salt between 4,900 and 5,200 feet). Also, relatively dense geologic formations are found between 3,400 and 3,900 ft (Bass Island Dolomite).

Table 3-2 contains the density differences (also termed 4D densities) and errors calculated for the three surveys. The density differences between the surveys are also presented in Figure 3-3 and Figure 3-4. Figure 3-3 presents data over the entire well and Figure 3-4 presents the data for the reef zone (Zone 1). Figure 3-3 displays the limited change in density in the upper portion of the well between the three surveys. In general, the data show relatively consistent gravity over the upper portion of the well (above 5,000 feet) between the three surveys performed in 2013, 2016, and 2018. This trend would be expected because no CO_2 injection or intrusion occurred in this area and limited perturbance to the geology likely occurred across these intervals during the monitoring period.

Near the reef (Figure 3-4), the differences in density (caused by the injection of CO_2) become apparent. Within the reef, the density typically increases between the 2013 and 2016 surveys from the injection of CO_2 and then decreases between the 2016 and 2018 surveys as CO_2 and oil are produced from the reef. Often, the 2018 density lies between the densities calculated from the 2013 and 2016 survey data, which is the expected result given the intermediate mass of CO_2 in the reef at the time of the 2018 survey.

Table 3-1. Borehole gravity densities for the 2013, 2016, and 2018 gravity surveys.

Station ID	MD2013 Zwld2013 (ft)	InvDen 2018 (g/cm3)	InvDen 2016 (g/cm3)	InvDen 2013 (g/cm3)
35	650.04	2.436	2.438	2.437
34	840.06	2.513	2.515	2.515
33	1176.07	2.624	2.626	2.626
32	1479.08	2.658	2.660	2.660
31	1805.09	2.670	2.670	2.672
30	2112.08	2.719	2.721	2.723
29	2358.08	2.452	2.451	2.458
28	2562.08	2.740	2.740	2.741
27	2946.08	2.662	2.662	2.663
26	3246.06	2.613	2.613	2.618
25	3432.05	2.830	2.832	2.832
24	3556.04	2.863	2.861	2.864
23	3698.03	2.782	2.781	2.785
22	3880.03	2.272	2.271	2.281
21	4098.03	2.282	2.281	2.286
20	4382.04	2.377	2.371	2.382
19	4508.04	2.373	2.368	2.382
18	4653.03	2.482	2.481	2.485
17	4846.06	2.288	2.286	2.294
16	5014.03	2.174	2.169	2.177
15	5176.02	2.473	2.462	2.496
14	5217.02	2.744	2.758	2.746
13	5247.02	2.786	2.792	2.800
12	5276.00	2.842	2.856	2.828
11	5305.99	2.687	2.715	2.703
10	5320.01	2.768	2.755	2.771
9	5349.99	2.710	2.721	2.703
8	5370.00	2.640	2.667	2.644
7	5390.01	2.631	2.654	2.630
6	5410.02	2.671	2.653	2.660
5	5430.04	2.682	2.712	2.684
4	5449.99	2.697	2.688	2.684
3	5480.03	2.695	2.704	2.696
2	5510.03	2.689	2.715	2.687
1	5540.03			

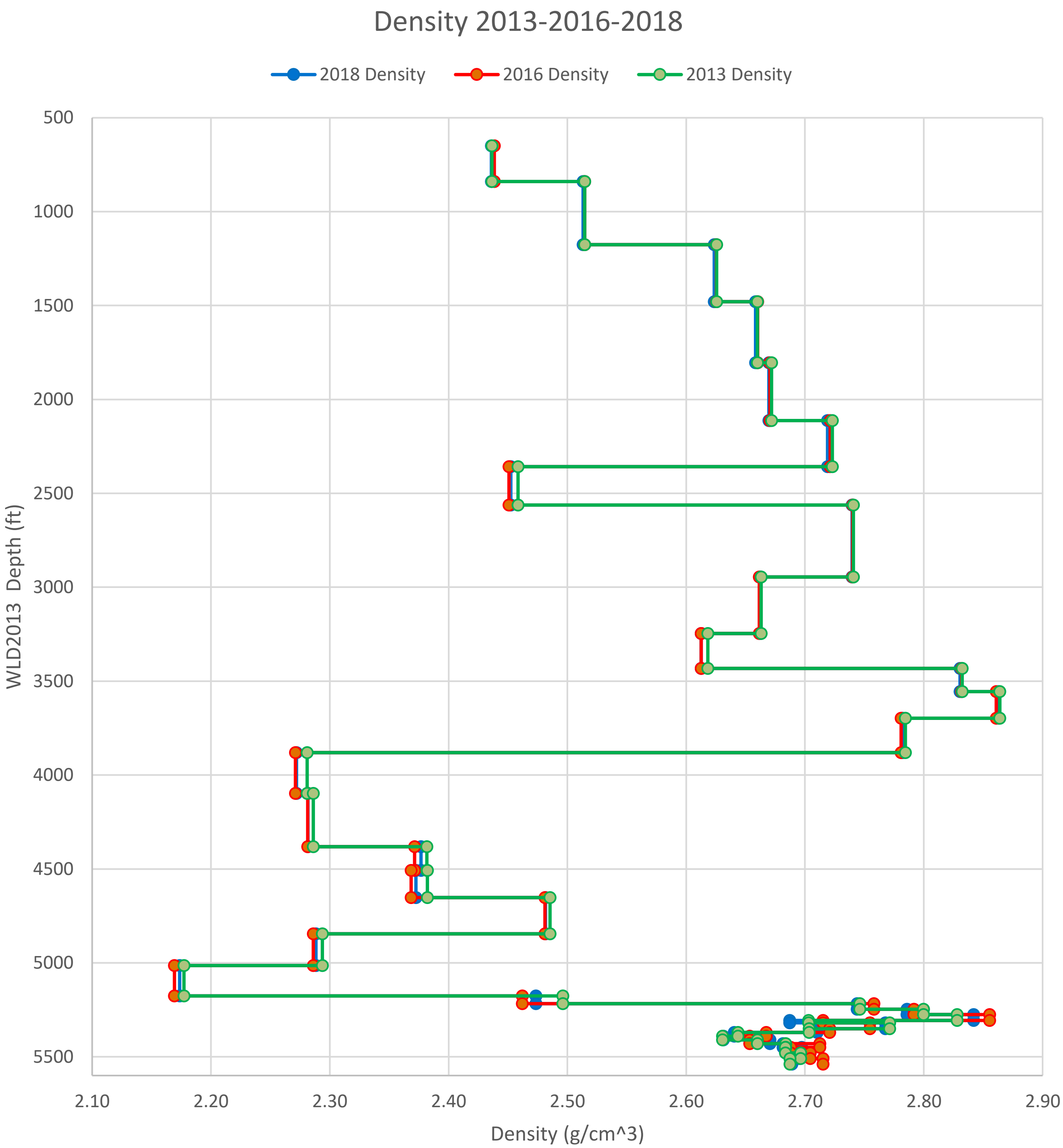

Figure 3-2. Borehole gravity densities from 2013, 2016, and 2018 gravity surveys.

Table 3-2. 4D Borehole gravity density difference signals and errors for the 2013, 2016, and 2018 surveys.

Station StnID	MD2013 Zwld2013 (ft)	4D Density 2016-2013 (g/cm3)	4D Dens Err 2016-2013 (g/cm3)	4D Density 2018-2013 (g/cm3)	4D Dens Err 2018-2013 (g/cm3)	4D Density 2018-2016 (g/cm3)	4D Dens Err 2018-2016 (g/cm3)
35	650.04	0.002	0.001	-0.001	0.001	-0.003	0.001
34	840.06	0.000	0.000	-0.002	0.001	-0.002	0.001
33	1176.07	0.000	0.001	0.000	0.001	0.000	0.001
32	1479.08	0.000	0.001	0.001	0.001	0.002	0.000
31	1805.09	-0.001	0.000	0.000	0.000	0.001	0.000
30	2112.08	-0.002	0.000	-0.001	0.000	0.001	0.001
29	2358.08	-0.003	0.001	-0.004	0.001	-0.001	0.001
28	2562.08	0.002	0.001	0.004	0.001	0.002	0.000
27	2946.08	0.003	0.001	0.005	0.001	0.002	0.000
26	3246.06	0.000	0.001	-0.003	0.001	-0.004	0.001
25	3432.05	-0.002	0.002	-0.001	0.002	0.001	0.001
24	3556.04	-0.004	0.001	0.001	0.002	0.005	0.001
23	3698.03	-0.004	0.001	-0.003	0.001	0.001	0.001
22	3880.03	0.003	0.001	-0.002	0.001	-0.005	0.000
21	4098.03	-0.003	0.001	-0.003	0.001	0.000	0.000
20	4382.04	-0.005	0.002	-0.003	0.002	0.002	0.001
19	4508.04	-0.009	0.001	-0.003	0.001	0.006	0.001
18	4653.03	-0.004	0.001	-0.001	0.001	0.003	0.001
17	4846.06	-0.003	0.002	-0.004	0.001	-0.001	0.002
16	5014.03	0.008	0.002	0.006	0.001	-0.002	0.002
15	5176.02	0.014	0.005	0.008	0.005	-0.007	0.002
14	5217.02	-0.021	0.007	-0.037	0.007	-0.016	0.003
13	5247.02	-0.012	0.008	-0.012	0.007	0.000	0.003
12	5276.00	0.019	0.007	0.012	0.006	-0.006	0.003
11	5305.99	-0.012	0.015	-0.037	0.016	-0.025	0.008
10	5320.01	-0.009	0.009	0.000	0.009	0.009	0.005
9	5349.99	0.006	0.011	0.009	0.011	0.003	0.007
8	5370.00	0.042	0.008	0.002	0.008	-0.039	0.006
7	5390.01	0.033	0.007	0.004	0.008	-0.029	0.005
6	5410.02	-0.013	0.007	0.002	0.007	0.015	0.005
5	5430.04	0.022	0.006	0.001	0.006	-0.022	0.005
4	5449.99	0.008	0.005	0.013	0.005	0.005	0.004
3	5480.03	0.006	0.006	0.000	0.006	-0.006	0.004
2	5510.03	0.023	0.005	0.004	0.005	-0.019	0.003
1	5540.03						

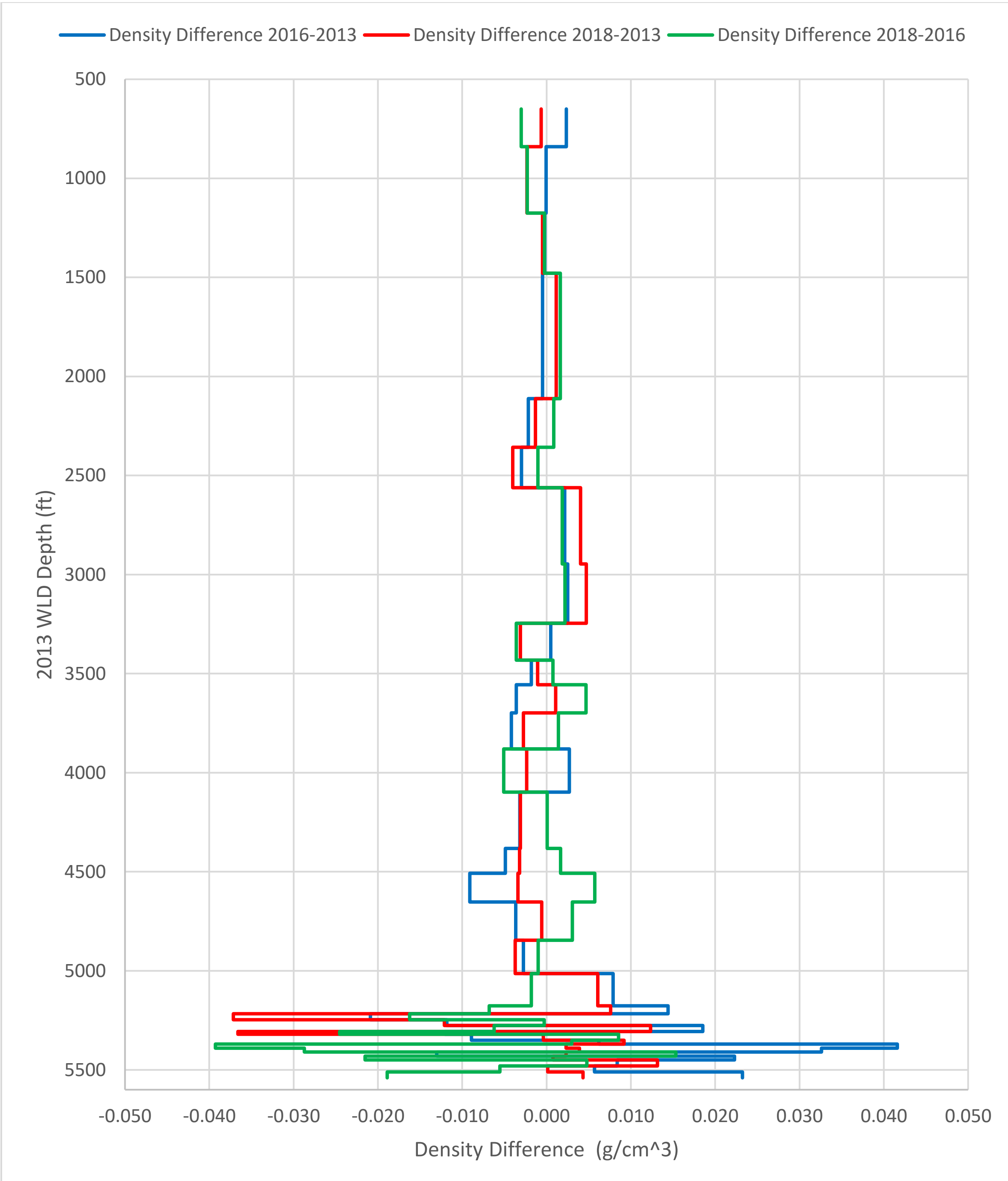

Figure 3-3. 4D Borehole gravity density differences (from gravity differences).

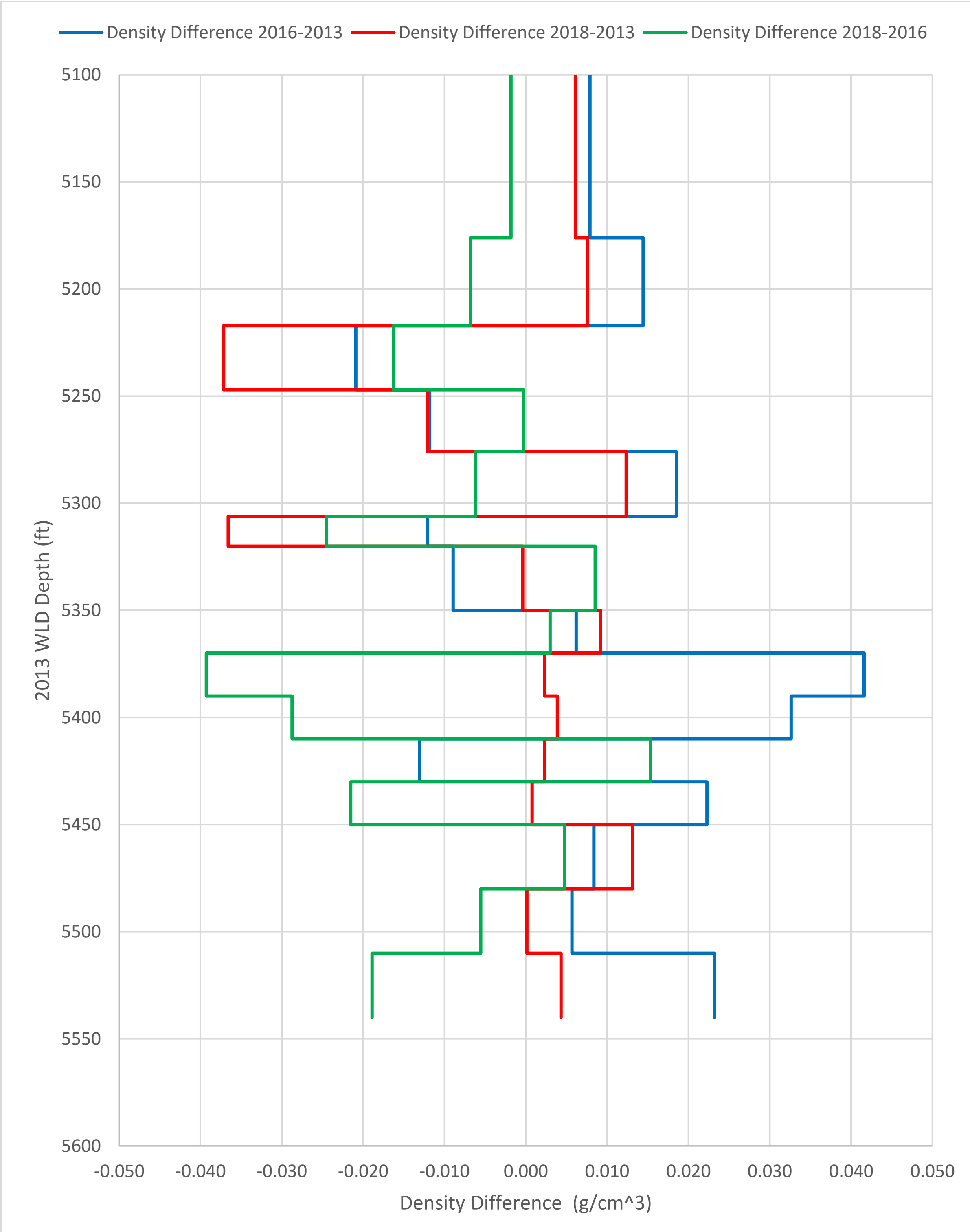

Figure 3-4. 4D Borehole Gravity Density Differences (Zoomed to Zone 1 only).

3.1.2 CO_2 Plume Imaging Using Forward Gravity Modeling

The goal of this approach is to determine where the CO_2 went in the reef after the injection, what is left after the withdrawal, and where it is located. In another words, this modelling will give an idea of the evolution of the CO_2 plume in three dimensions with time. Pacific Northwest National Laboratory (PNNL) completed this 3D forward modelling, using GRAV3D v5.0 (UBC-Geophysical Inversion Facility, 2017), of the density anomalies responsible for the difference in gravity signal observed between the 2016 Survey and the 2013 Survey and between the 2018 Survey and the 2016 Survey, as well. The model used the static earth geological model of the reef prepared by Battelle as well as the estimated saturations of CO_2, oil, and water in each formation in the different formations before and after the injection of CO_2.

Figure 3-5 and Figure 3-6 illustrate the structure of the reservoir that was modeled by Battelle and the location of the L-M 1-33 well (marked with symbol to the left of Dover 33 label) and borehole gravity stations, respectively.

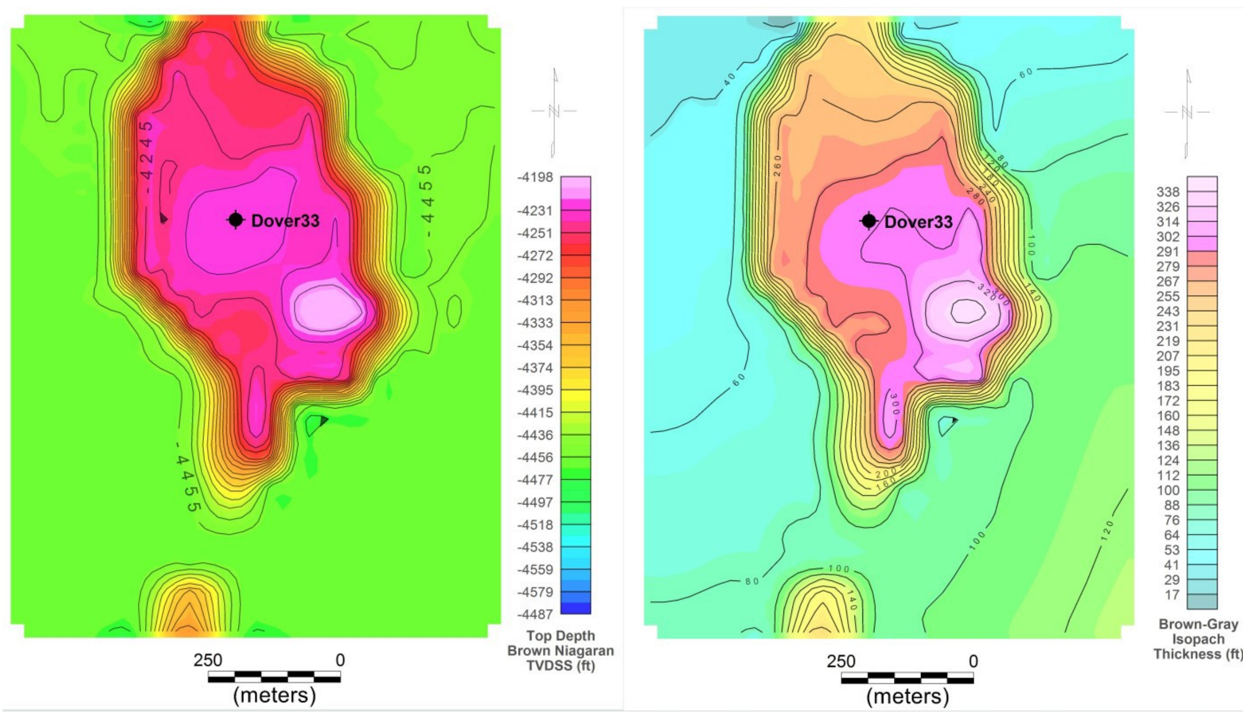

Figure 3-5. Left: Structure contour map of the top of the Brown Niagaran Formation. Right: Brown Niagaran to Gray Niagaran isopach map. Structural grids of these formations were provided by Battelle (from Hare et al., 2017).

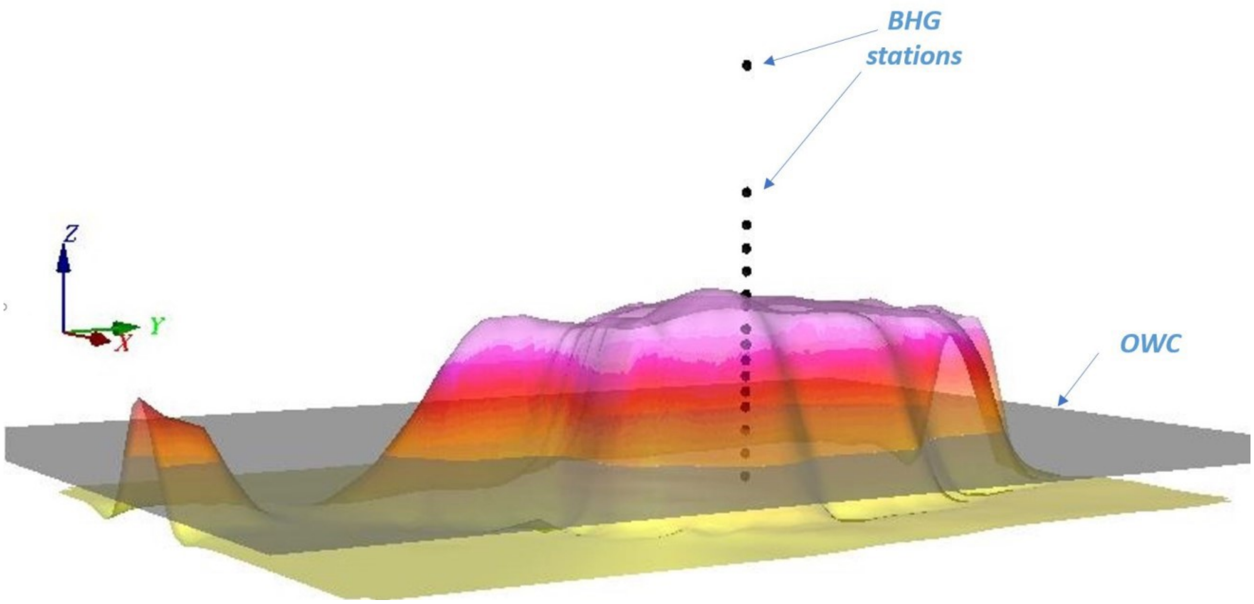

Figure 3-6. Three-dimensional perspective diagram of the reef showing the location of the borehole gravity stations along the well trajectory through the reef. The gray plane is the location of the indicated Oil Water Contact (OWC) (5,470 ft MD). View in this image is from southeast toward northwest. (from Hare et al., 2017).

The reservoir static earth model (Figure 3-7) has the following characteristics:

- Surface elevation = 344.94 m
- xmin = 612,990 m; xmax = 613,666 m; difference = 676 m
- ymin = 498,900 m; – ymax = 500,100 m; difference = 1,200 m
- Height in terms of elevation (m): zmin = -1,385.52 m; zmax = -1,268.35 m; difference = 117.17 m (elevation)
- Height in terms of depth (m): zmin = 1,613.29 m; zmax = 1,730.46 m; difference = 117.17 m (depth)
- Height in terms of depth (ft): zmin = 5,293 ft; zmax = 5,677 ft; difference = 384.4 ft (depth)
- Total porous rock volume = 24,824,844 m^3
- Total volume of porous space = 1,067,468 m^3 with average porosity = 0.043
- Maximum permeability = 40 mD

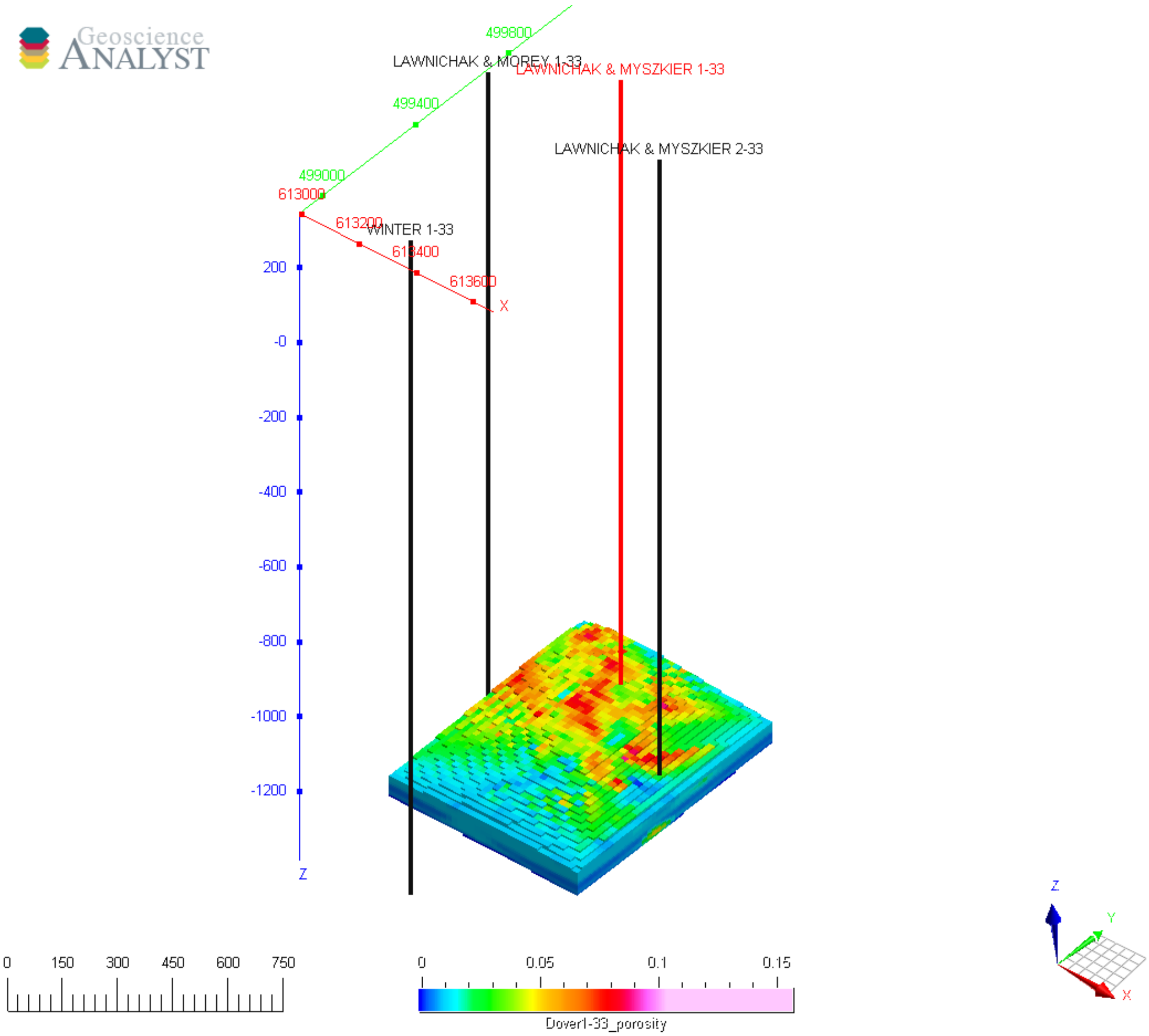

Figure 3-7. Three-dimensional perspective diagram of the static earth model prepared by Battelle and used in the present study.

3.1.3 Forward Modeling

The main approach adopted in this study is based on the forward modeling of the time-lapse gravity anomalies observed in the L-M 1-33 well. To make this forward modeling possible, a time-lapse density model based on the reservoir model presented in Section 3.3.2 is required. In the absence of density values and of multiphase flow modelling corresponding to the periods of injection and production, the porosity and permeability distribution in the reef was used as a way of constraining the density distribution. This approach is to progressively fill the empty porous space of the 3D reef model starting from the injection point until a maximum distance from the well is reached while the permeability stays greater or equal to a defined threshold, (for example only connected cells with permeability >6 mD and within a maximum radius of 200 meters from the well were considered). By varying these parameters in each range, a series of time-lapse density grids (“CO_2 plume”) were obtained that could then be used to generate the gravity anomaly to be compared to the observed time-lapse values. For example, by setting the minimum permeability equal to 0, 2, 4, 8, 16 and 32 mD and the maximum distance equal to 100, 200, 300, 400, 500 and 600 meters, 36 realizations of the CO_2 plume and thus 36 modeled gravity profiles were obtained (Table 3-3). The modeling algorithm stops when the mass of CO_2 in the reef reaches the total injected CO_2 mass (positive) during 2013-2016 period or the total withdrawn CO_2 mass (negative) during the 2016-2018 period is reached. This approach was conducted for the two periods and 72 realizations were analyzed. The results are very encouraging because for cases that make the most sense physically, a good fit is obtained between the corresponding modeled gravity anomalies and observed anomalies.

Table 3-3. Various scenarios used in the forward modeling.

2013-2016 Injection			2016-2018 Production		
K min (mD)	Max CO_2 Plume Radius (m)	Injected CO_2 mass (tons)	K min (mD)	Max CO_2 Plume Radius (m)	Produced CO_2 mass (tons)
0	100	109950	0	100	-73593
0	200	264544	0	200	-142993
0	300	264523	0	300	-142993
0	400	264523	0	400	-142993
0	500	264523	0	500	-142993
0	600	264523	0	600	-142993
2	100	72653	2	100	-48628
2	200	240023	2	200	-143023
2	300	264519	2	300	-143028
2	400	264519	2	400	-143028
2	500	264519	2	500	-143028
2	600	264519	2	600	-143028
4	100	48074	4	100	-32177
4	200	164506	4	200	-110109
4	300	264576	4	300	-143048
4	400	264553	4	400	-143048
4	500	264553	4	500	-143048
4	600	264553	4	600	-143048
8	100	26736	8	100	-17895
8	200	88820	8	200	-59450
8	300	167511	8	300	-112120
8	400	254996	8	400	-143050
8	500	264577	8	500	-143009
8	600	264577	8	600	-143009
16	100	5457	16	100	-3652
16	200	20215	16	200	-13531
16	300	53318	16	300	-35687
16	400	85786	16	400	-57419
16	500	96215	16	500	-64400
16	600	96850	16	600	-64824

In the absence of knowledge of the variations of the CO_2 saturation, which could only be estimated by multiphase modelling, a saturation of 0.8, which is the maximum value measured at the bottom well at the end of the injection period, was used. Note, taking a lower value of the saturation would increase the diameter of the CO_2 plume. Also, it must be noted that a higher permeability threshold tends to spread the

CO_2 farther away from the well because the flow paths for CO_2 are limited to high permeability channels. Keeping the minimum permeability at zero implies considering all the cells of the model with a permeability greater than zero with the consequence of filling all the pores close to the well more quickly and thus keeping the CO_2 plume at a minimum size.

3.1.4 CO_2 Injection Period (2013-2016) Model Results

Figure 3-8 presents the results for a chosen set of realizations. The best fits are obtained without imposing a minimum permeability (i.e., k-min > 0). The model with a plume radius of 300 m appears to provide the optimal fit for the anomaly at the top of the reef or just above it. Note, the anomaly at 5,000 ft (above the reef) is not perfectly explained by this model and this should be the focus of the 3D inversion model that will be performed later. Figure 3-9 presents the corresponding time-lapse density distribution in the reef and it is important to note that most of the CO_2 is concentrated in the lower part of the reef.

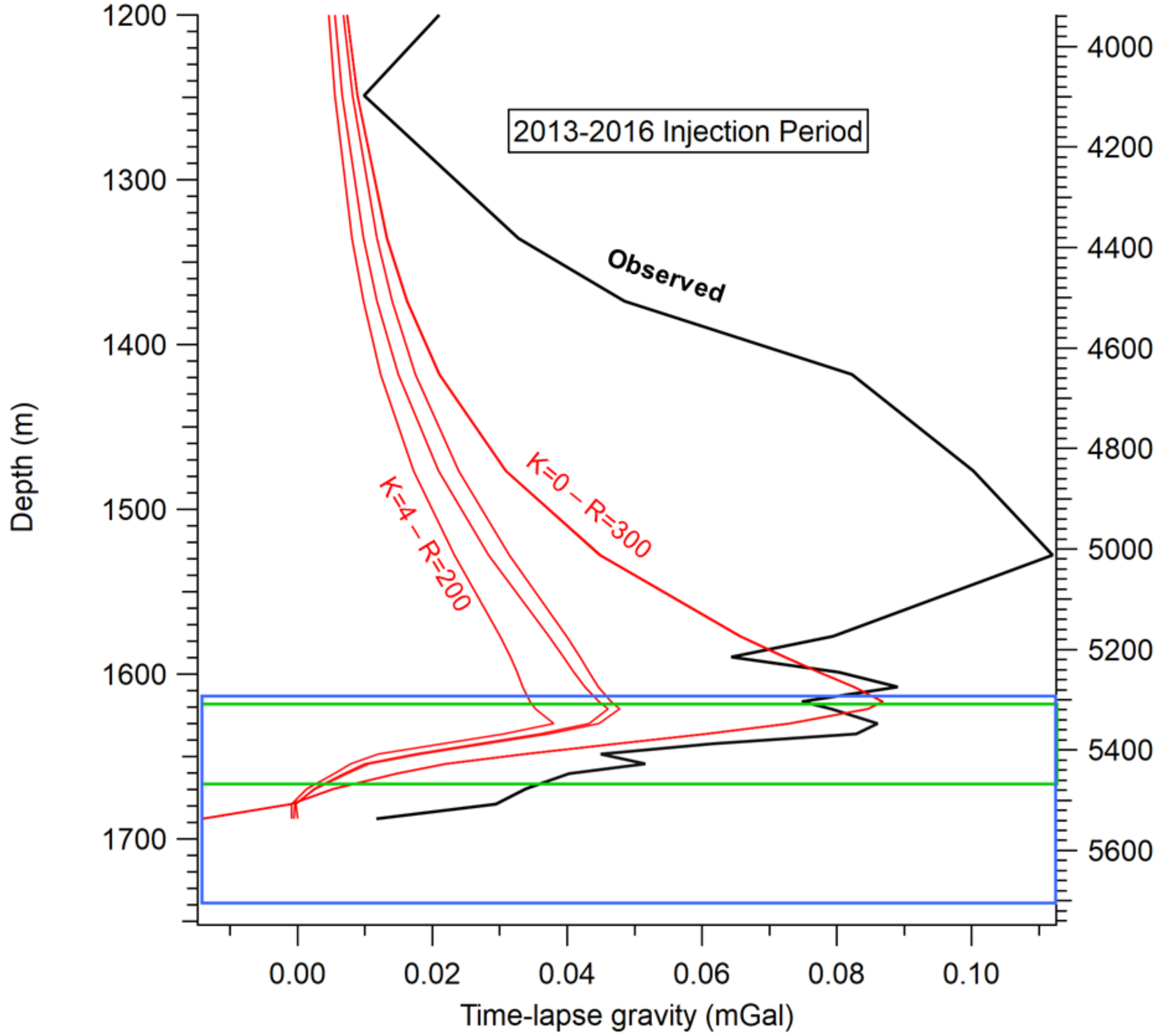

Figure 3-8. 2013-2016 injection period: comparison of forward models (in red) to observed time-lapse gravity profile (in black) and the inversion model (in green). The blue box corresponds to the reef reservoir model and the green box to the perforated interval. The best fit corresponds to the case K=0 and R=300 m (see text).

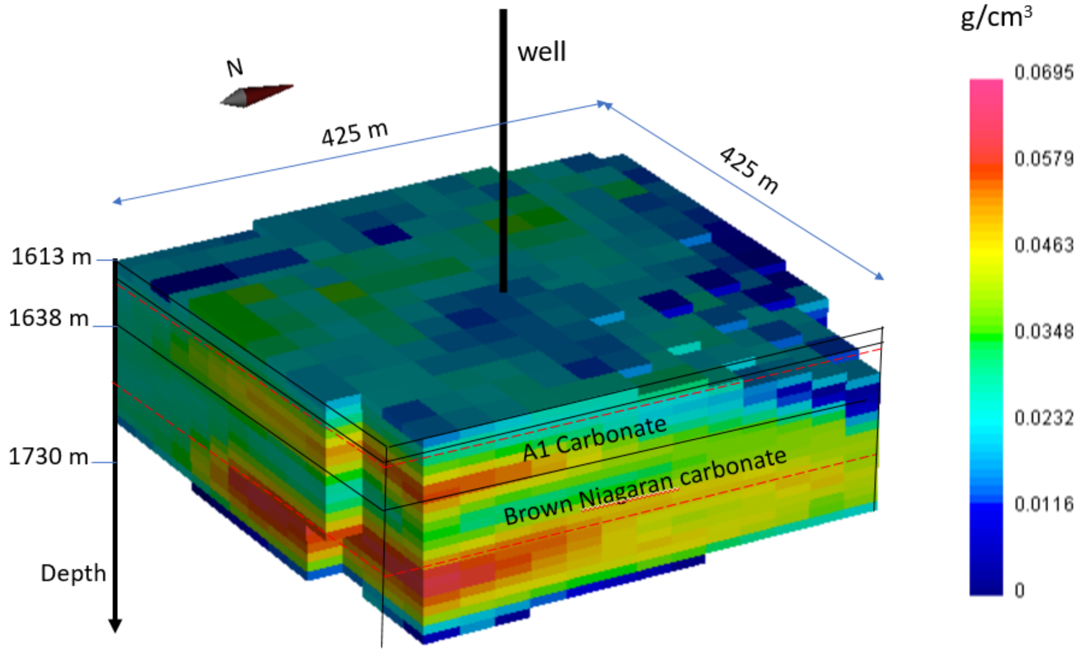

Figure 3-9. 2013-2016 injection period: three-dimensional perspective diagram of the modelled time-lapse density that represents the CO_2 plume in the reef for the best fitting solution K=0- R=300. The vertical black line represents the L-M 1-33 well. The horizontal black lines are the limits between the main geological units and the depth interval between the two horizontal red dashed lines is the perforated interval of the injection well.

3.1.5 Oil/CO_2 Production Period (2016-2018) Model Results

Figure 3-10 presents the results for a chosen set of realizations during the p roduction phase (2016-2018). The best fits are obtained without imposing a minimum permeability (k = 0) and among them, the plume with a radius of 300 m provides the optimal fit for the anomaly at the top of the reef or just above it, as observed for the injection period. Note that the anomaly at 4,800 ft, although better fitted by this model than in the case of the injection, is still not completely explained. Figure 3-11 presents the corresponding time-lapse density distribution in the reef for the production period. As modeled in the injection period, the maximum decrease of CO_2 density during the production period is concentrated in the lower part of the reef where the porosity is maximum.

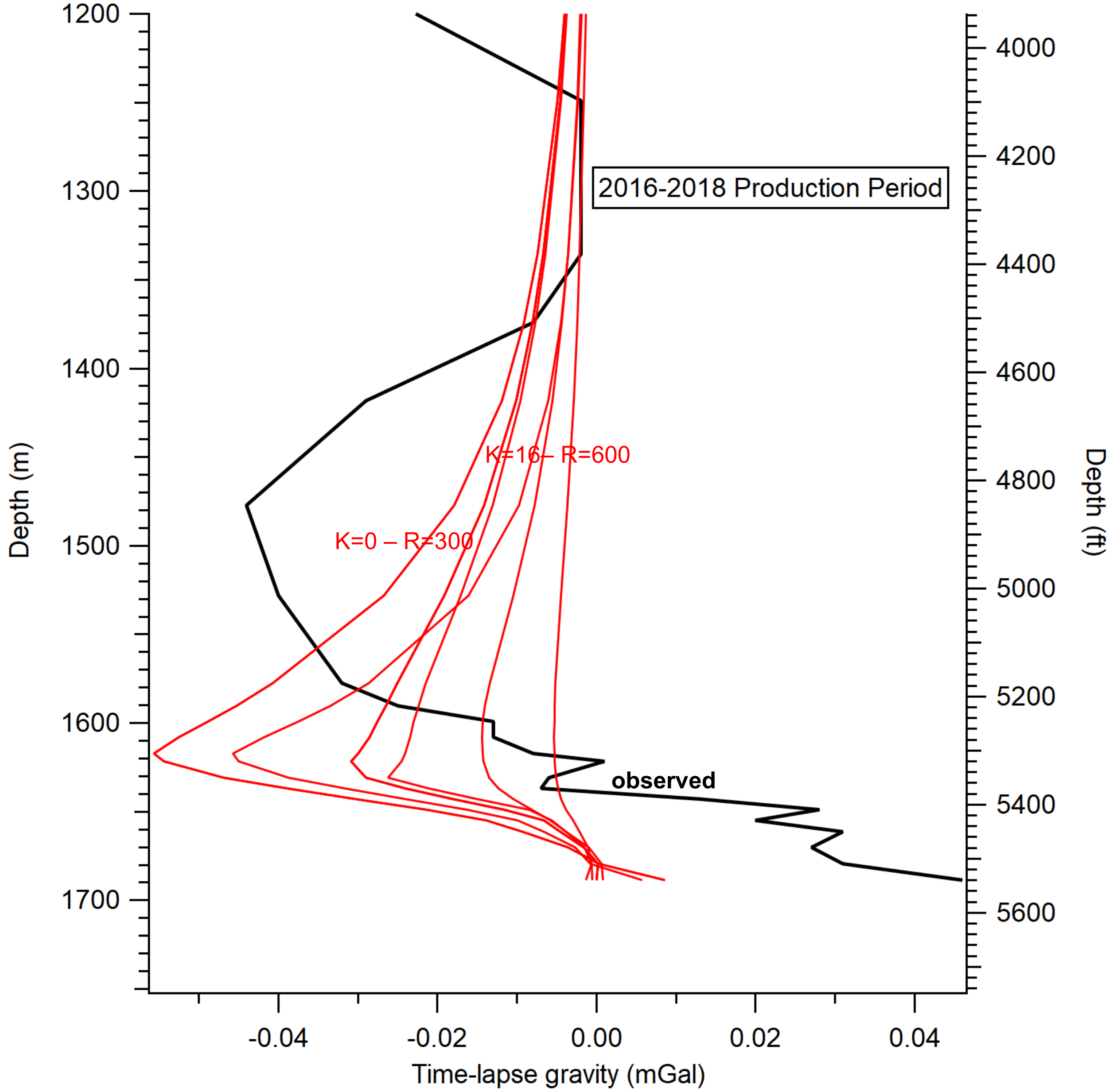

Figure 3-10. 2016-2018 production period: comparison of forward models (in red) to observed time-lapse gravity profile (in black) and the inversion model (in green). The best fit corresponds to the case K=0 and R=300 m (see text).

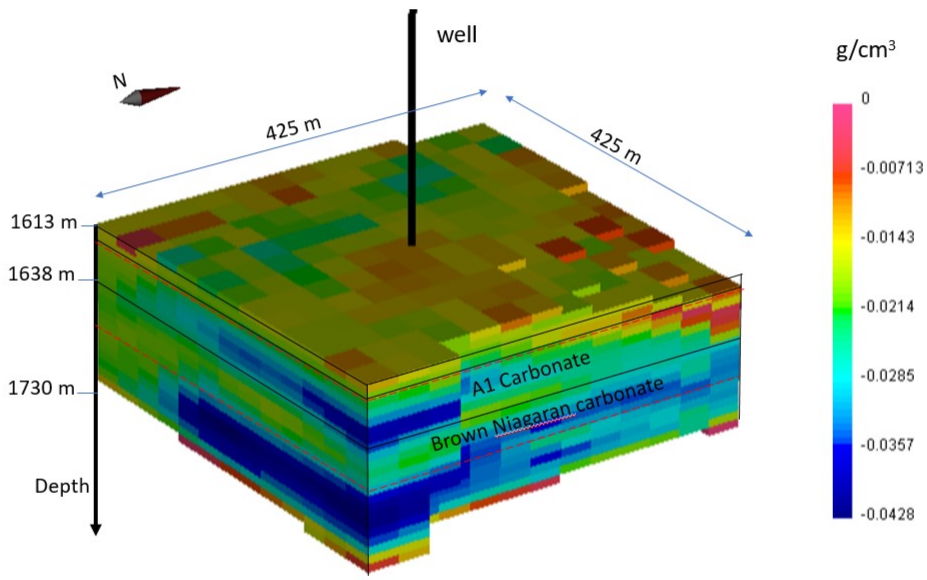

Figure 3-11. 2016-2018 production period: three-dimensional perspective diagram of the modelled time-lapse density in the reef for the best fitting solution K=0- R=300. The vertical black line represents the L-M 1-33 well. The horizontal black lines are the limits between the main geological units and the depth interval between the two horizontal red dashed lines is the perforated interval of the injection well.

4.0 Summary and Conclusions

The borehole gravity data collected during the 2013, 2016, and 2018 surveys performed by Tellus Gravity represent the state-of-the-art in terms of data acquisition and pre-processing. The depth control in particular was meticulously conducted. Their quality and the low level of uncertainty make them useful for delineating the CO_2 plume position over time deployment and the oil sweeping extent and mechanisms in the Dover 33 reef. The following preliminary conclusions can be drawn:

- The time-lapse Bouguer gravity plots clearly show the effects of the changing mass of CO_2 within the reservoir, consistent with increasing mass from 2013 to 2016 and a decreasing mass from 2016 to 2018.
- The positive anomaly after the injection period in 2016 is likely due to the filling of the reef reservoir by CO_2. The best fitting forward models correspond to CO_2 mainly being stored in the central and lower portions of the reef. The forward modeling method allows precise mapping of the areas of the reservoir that received most of the injected CO_2 and which zones are likely to have received less CO_2. The results of preliminary inversion models (not represented here) confirm partly the forward modelling for this initial injection period.
- For the production period, the time-lapse gravity anomaly corresponds clearly to the withdrawal of roughly 136,000 tons of CO_2. It is, however, not completely explained by the forward models presented and this could be due to the migrations of fluids in the reservoir not considered in this approach.

Overall, the field data collected in this study shows a strong correlation between the reservoir CO_2 injection and production operations. The changes in gravity and density, generally correspond with the injection zone and the most pronounced changes are in the reservoir, rather than in the overlying 5,000+ feet. This indicates that borehole gravity can be a useful tool in monitoring CO_2 injection in depleted oil fields, including under CO_2-EOR conditions. This technique could also be used for monitoring injection in saline reservoirs, given that the basic mechanisms of increasing gravity/density with injection still hold. The cost of the tool deployment is also relatively low, potentially less than $100,000 per monitoring event. This could be further reduced through standardization and more widespread use of the technology in commercial applications. The relative value of the borehole gravity over the other options, such as pressure, temperature, and emerging distributed fiber-optic systems remains to be seen. Some challenges include the need for precise repetition of field procedures and measurement locations. The complexity of CO_2-EOR operations overtime in fields such as Dover 33 is difficult to fully incorporate into the analyses or modeling. Furthermore, with a single monitoring well used in this study, it is difficult to evaluate lateral changes in the CO_2 plume. Perhaps if the tool is used in multiple wells in the project area, a more detailed plume distribution could be developed.

5.0 References

AhmadZamri, A. F., Musgrove, F. W., Bridle, I. M., Angelich, M. T., and VandenBosch, R., 2009, Successful reservoir monitoring with 4D microgravity at Ras Laffan, State of Qatar: International Petroleum Technology Conference, Doha, Qatar. IPTC paper 13640.

Appriou D. and A. Bonneville, Monitoring Carbon Storage Sites with Time-Lapse Gravity Surveys in Geophysical Monitoring for Geologic Carbon Utilization and Storage, L. Huang Ed., American Geophysical Union, in press.

Beyer, L. A., 1983, Borehole Gravity Surveys: Theory, Mechanics, and Nature of Measurements. U.S. Geological Survey Open File Report, No. 83-76.

Black A.J. and E. Mann, 2018 Borehole Gravity Survey of the Lawnichak-Myszkier 1-33 Well, Ostego County, Michigan, Part 1: Data Processing and Presentation (Preliminary), Report, Tellus Gravity LLC, October 3, 2018.

Black, A., Hare, J., MacQueen, J., 2016, Borehole gravity monitoring in the Aquistore CO_2 Sequestration Well: 86th Annual International Meeting, Exp. Abstr., SEG, Dallas, Texas.

Brady, J. L., Hare, J. L., Ferguson, J. L., Seibert, J. E., Klopping, F. J., Chen, T., and Niebauer, T., 2006, Results of the world's first 4D microgravity surveillance of a waterflood- Prudhoe Bay, Alaska: SPE Annual Technical Conference and Exhibition, San Antonio, Texas, SPE 101762.

Eiken, O., Stenvold, T., Zumberge, M., Aines, H., and Sasegawa, G., 2008, Gravimetric monitoring of gas production from the Troll field, Geophysics, 73, no. 6, WA149-WA154.

Haagsma, A., Rine, M., Sullivan, C., Conner, A., Kelley, M., Modroo, A., Larsen, G., and Gupta, N., 2017, Static earth modeling of diverse Michigan Niagara reefs and implications for CO_2 storage: Energy Procedia no. 114, pp. 3353-3363.

Haagsma, A., Conner, A., Cotter, Z., Grove, B., Main, J., Scharenberg, M., Larsen, G., Raziperchikolaee, S., Goodman, W., Sullivan, C., and Gupta, N. (2020). Geologic Characterization for CO_2 Storage with Enhanced Oil Recovery in Northern Michigan. MRCSP topical report prepared for DOE-NETL project DE-FC26-05NT42589, Battelle Memorial Institute, Columbus, OH.

Hare and Black, 2015, Evolution of microgravity surveys for reservoir monitoring, Monitoring giant carbonate fields: Fad or future, Exp. Abstr., SEG/SPE Workshop, Abu Dhabi, UAE.

Hare, J. L., Ferguson, J. F., Aiken, C. L. V., and Brady, J. L., 1999, The 4D microgravity method for waterflood surveillance: A model study for the Prudhoe Bay reservoir, Alaska: Geophysics, 64, 78-87.

Hare, J., A. Black, J. MacQueen, and T. Niebauer, 2016 Borehole Gravity Survey of the Lahwnichak-Myskier 1-33 Well, Ostego County, Michigan, MGL-BHG-2016-005 Report, Micro-g LaCoste, Inc., February 2017.

Kabirzadeh, H., Kim, J., and Sideris, M., 2016, Micro-gravimetric monitoring of geological CO_2 reservoirs, International Journal of Greenhouse Gas Control, 56, pp. 187-193.

Krahenbuhl, R. and Li, Y., 2012, Time-lapse gravity: A numerical demonstration using robust inversion and joint interpretation of 4D surface and borehole data, Geophysics, 77, no. 2, pp. G33-G43.

Krahenbuhl, R., Li, Y., and Nind, C., 2012, The benefit of borehole gravity in horizontal monitoring wells for time-lapse applications: 83rd Annual International Meeting, Exp. Abstr., SEG, Las Vegas, Nevada.

LaFehr, T. R. (1983), Rock density from borehole gravity surveys, GEOPHYSICS, 48(3), 341-356, doi:10.1190/1.1441472.

MacQueen, J. D., 2007, High-resolution density from borehole gravity data, Exp. Abstr., 77th Annual International Meeting, San Antonio, Texas.

Nind, C., P. D. J. MacQueen, R. Wasylechko, M. Chemam, and C. Nackers (2013), Gravilog: An update on the development and use of borehole gravity for mining exploration, in ASEG Extended Abstracts 2013: 23rd Geophysical Conference, edited, pp. 1-5, doi:10.1071/ASEG2013ab048.

Rim, H., and Li, Y., 2015, 4D inversion of borehole gravity data for monitoring fluid fronts: 24th International Geophysical Conference and Exhibition, Exp. Abstr., ASEG-PESA, Perth, Western Australia.

Robbins, S. L. (1989), Borehole Gravimetry Reviews Rep., U.S. Geological Survey.

Van Gelderen, M., Haagmans, R., and Milker, M., 1999, Gravity changes and natural gas extraction in Groningen: Geophysical Prospecting, 47, 979-993.

Van Popta, J., Heywood, J.T., Adams, S.J., and Bostock, D. R., 1990, Use of borehole gravimetry for reservoir characterization and fluid saturation monitoring: Proceedings of the 7th European Offshore Petroleum Conference (Europec '90), The Hague, Netherlands.

Appendix A.

Survey Data

Appendix A. Survey Data

Table A-1. Reprocessed station gravity and errors for the 2013 survey.

Station	TVD (ft)	Station WLD (ft)	Gravity (mGals)	Occupations	Station Sigma (mGal)	Accuracy (mGals)
35	650.0	650.0	3275.883	3	0.013	0.007
34	840.0	840.0	3281.922	3	0.010	0.005
33	1175.8	1176.1	3291.915	3	0.002	0.001
32	1478.6	1479.1	3300.069	2	0.012	0.009
31	1804.5	1805.1	3308.559	2	0.006	0.004
30	2111.5	2112.1	3316.465	3	0.005	0.003
29	2357.5	2358.1	3322.478	3	0.004	0.002
28	2561.4	2562.1	3328.854	3	0.016	0.009
27	2945.4	2946.1	3338.064	3	0.014	0.008
26	3245.4	3246.0	3345.862	6	0.015	0.006
25	3431.4	3432.0	3350.921	3	0.015	0.009
24	3555.3	3556.0	3353.598	3	0.008	0.004
23	3697.3	3698.0	3356.557	3	0.013	0.007
22	3879.3	3880.0	3360.715	3	0.014	0.008
21	4097.3	4098.0	3368.531	3	0.020	0.011
20	4381.3	4382.0	3378.643	3	0.019	0.011
19	4507.2	4508.0	3382.833	3	0.013	0.007
18	4652.2	4653.0	3387.645	3	0.009	0.005
17	4845.1	4846.0	3393.531	3	0.016	0.009
16	5012.8	5014.0	3399.484	3	0.009	0.005
15	5174.5	5176.0	3405.700	7	0.014	0.005
14	5215.4	5217.0	3406.977	4	0.016	0.008
13	5245.3	5247.0	3407.662	4	0.013	0.006
12	5274.3	5275.9	3408.311	4	0.018	0.009
11	5304.2	5305.9	3408.959	4	0.007	0.003
10	5318.2	5319.9	3409.300	4	0.019	0.010
9	5348.1	5349.9	3410.002	4	0.015	0.008
8	5368.1	5369.9	3410.495	4	0.013	0.006
7	5388.0	5389.9	3411.034	4	0.005	0.003
6	5408.0	5410.0	3411.575	4	0.012	0.006
5	5428.0	5430.0	3412.093	4	0.003	0.001
4	5447.9	5449.9	3412.598	4	0.008	0.004
3	5477.9	5480.0	3413.365	4	0.010	0.005
2	5507.8	5510.0	3414.118	4	0.013	0.007
1	5537.8	5540.0	3414.877	3	0.005	0.003

Table A-2. Station gravity and errors for the 2016 survey.

Station	TVD (ft)	Station WLD (ft)	Gravity (mGals)	Occupations	Station Sigma (mGal)	Accuracy (mGals)
39	10.5	10.5	433.094	1	0.000	0.000
38	22.1	22.1	4334.140	1	0.000	0.000
37	34.1	34.1	4334.884	1	0.000	0.000
36	240.5	240.5	4342.602	1	0.000	0.000
35	660.5	660.5	4357.111	3	0.003	0.002
34	850.6	850.6	4363.138	3	0.003	0.002
33	1186.3	1186.6	4373.131	3	0.007	0.004
32	1489.1	1489.6	4381.287	3	0.005	0.003
31	1815.2	1814.8	4389.782	3	0.005	0.003
30	2122.0	2122.6	4397.694	3	0.006	0.003
29	2368.0	2368.6	4403.720	3	0.005	0.003
28	2571.5	2572.1	4410.112	3	0.011	0.006
27	2954.0	2954.6	4419.301	3	0.011	0.006
26	3252.8	3253.4	4427.080	5	0.007	0.003
25	3438.1	3438.7	4432.136	3	0.005	0.003
24	3561.7	3562.4	4434.819	3	0.005	0.003
23	3703.6	3704.3	4437.791	3	0.003	0.002
22	3885.3	3886.0	4441.968	3	0.004	0.003
21	4101.8	4102.5	4449.768	3	0.005	0.003
20	4385.2	4385.9	4459.904	3	0.005	0.003
19	4510.8	4511.6	4464.109	3	0.006	0.003
18	4655.3	4656.1	4468.955	3	0.009	0.005
17	4847.8	4848.7	4474.859	3	0.009	0.005
16	5015.1	5016.3	4489.824	2	0.021	0.015
15	5175.1	5176.6	4487.007	5	0.006	0.003
14	5215.6	5217.2	4488.269	6	0.004	0.002
13	5245.3	5246.9	4488.970	4	0.005	0.003
12	5274.2	5275.9	4489.628	4	0.006	0.003
11	5304.3	5306.0	4490.262	4	0.004	0.002
10	5318.2	5320.0	4490.606	4	0.004	0.002
9	5348.2	5350.0	4491.316	3	0.008	0.004
8	5368.1	5370.0	4491.806	4	0.006	0.003
7	5388.1	5390.0	4492.323	4	0.003	0.002
6	5408.1	5410.0	4492.848	4	0.005	0.002
5	5428.0	5430.0	4493.372	4	0.004	0.002
4	5448.0	5450.0	4493.866	3	0.006	0.003
3	5477.9	5480.0	4494.627	4	0.005	0.003
2	5507.9	5510.0	4495.375	4	0.004	0.002
1	5537.9	5540.1	4496.117	3	0.004	0.002

Table A-3. Station gravity and errors for the 2018 survey.

Station	TVD (ft)	WLD (ft)	Gravity (mGals)	Occupations	Station Sigma (mGals)	Accuracy (mGals)
37	23.56	23.56	4413.588	1	0.000	0.000
36	229.96	230.02	4421.713	1	0.000	0.000
35	661.58	661.64	4436.691	3	0.011	0.006
34	851.60	851.76	4442.733	3	0.010	0.006
33	1187.64	1187.87	4452.746	3	0.010	0.006
32	1490.11	1490.58	4460.903	3	0.006	0.003
31	1815.15	1815.79	4469.384	3	0.006	0.003
30	2121.29	2122.00	4477.288	3	0.008	0.005
29	2366.66	2367.38	4483.309	3	0.002	0.001
28	2570.46	2571.18	4489.706	3	0.004	0.002
27	2952.08	2952.88	4498.876	3	0.000	0.000
26	3250.52	3251.06	4506.638	6	0.004	0.002
25	3436.39	3436.95	4511.712	6	0.004	0.002
24	3559.87	3560.44	4514.392	6	0.010	0.004
23	3701.68	3702.03	4517.347	3	0.012	0.007
22	3883.19	3883.53	4521.518	3	0.002	0.001
21	4100.48	4100.83	4529.346	3	0.001	0.001
20	4383.95	4384.34	4539.481	3	0.005	0.003
19	4509.93	4510.34	4543.682	3	0.001	0.001
18	4654.17	4654.63	4548.506	3	0.002	0.001
17	4846.40	4846.96	4554.395	3	0.004	0.002
16	5014.06	5014.83	4560.364	3	0.002	0.001
15	5174.69	5176.02	4566.555	8	0.004	0.002
14	5215.63	5217.02	4567.824	8	0.005	0.002
13	5245.57	5247.02	4568.537	8	0.005	0.002
12	5274.32	5276.00	4569.196	5	0.001	0.001
11	5304.26	5305.99	4569.834	4	0.006	0.003
10	5318.25	5320.01	4570.187	5	0.009	0.004
9	5348.16	5349.99	4570.890	5	0.007	0.003
8	5368.13	5370.00	4571.378	5	0.007	0.003
7	5388.10	5390.01	4571.916	5	0.008	0.003
6	5408.07	5410.02	4572.455	5	0.005	0.002
5	5428.10	5430.04	4572.972	5	0.007	0.003
4	5447.96	5449.99	4573.477	5	0.004	0.002
3	5478.02	5480.03	4574.234	5	0.007	0.003
2	5507.85	5510.00	4574.986	5	0.006	0.003
1	5537.81	5540.00	4575.743	5	0.005	0.002

Table A-4. Apparent densities from 2013 Survey.

Station ID	TVD (ft)	WLD (ft)	Conventional Density (g/cm3)	Sigma Conv Density (g/cm3)	Inversion Density (g/cm3)	Sigma Inv Density (g/cm3)
35	650.0019	650.0347	2.435	0.002	2.437	0.002
34	840.0128	840.0488	2.515	0.001	2.515	0.001
33	1175.783	1176.059	2.626	0.001	2.626	0.001
32	1478.594	1479.06	2.660	0.001	2.660	0.001
31	1804.502	1805.063	2.672	0.001	2.672	0.002
30	2111.477	2112.058	2.723	0.001	2.723	0.001
29	2357.455	2358.052	2.457	0.002	2.458	0.002
28	2561.442	2562.052	2.741	0.001	2.741	0.001
27	2945.424	2946.05	2.663	0.001	2.663	0.001
26	3245.384	3246.017	2.616	0.002	2.618	0.002
25	3431.369	3432.012	2.835	0.003	2.832	0.003
24	3555.337	3555.994	2.865	0.002	2.864	0.002
23	3697.327	3697.987	2.787	0.002	2.785	0.002
22	3879.316	3879.982	2.278	0.002	2.281	0.002
21	4097.312	4097.982	2.288	0.002	2.286	0.002
20	4381.285	4381.991	2.379	0.004	2.382	0.004
19	4507.232	4507.983	2.382	0.002	2.382	0.002
18	4652.178	4652.972	2.487	0.002	2.485	0.002
17	4845.125	4846.004	2.292	0.002	2.294	0.002
16	5012.803	5013.971	2.177	0.002	2.177	0.002
15	5174.465	5175.957	2.460	0.009	2.496	0.007
14	5215.383	5216.958	2.787	0.013	2.746	0.009
13	5245.33	5246.96	2.803	0.014	2.800	0.009
12	5274.253	5275.937	2.834	0.011	2.828	0.008
11	5304.181	5305.923	2.730	0.026	2.703	0.01
10	5318.18	5319.948	2.762	0.016	2.771	0.008
9	5348.098	5349.928	2.716	0.019	2.703	0.01
8	5368.068	5369.941	2.626	0.013	2.644	0.009
7	5388.035	5389.944	2.621	0.012	2.630	0.008
6	5408.008	5409.957	2.667	0.012	2.660	0.008
5	5427.992	5429.98	2.688	0.009	2.684	0.008
4	5447.903	5449.927	2.680	0.008	2.684	0.007
3	5477.883	5479.963	2.699	0.011	2.696	0.008
2	5507.84	5509.966	2.689	0.01	2.687	0.007
1	5537.79	5539.959				0.007

Table A-5. Apparent densities from 2016 Survey.

Station ID	TVD (ft)	WLD (ft)	Conventional Density (g/cm3)	Sigma Conv Density (g/cm3)	Inversion Density (g/cm3)	Sigma Inv Density (g/cm3)
39	10.5	10.5	0.161	0.024	0.286	0.022
38	22.1	22.1	1.246	0.023	1.253	0.021
37	34.1	34.1	2.216	0.001	2.213	0.001
36	240.5	240.5	2.327	0.000	2.327	0.001
35	660.5	660.5	2.438	0.001	2.438	0.001
34	850.6	850.6	2.515	0.001	2.515	0.001
33	1186.3	1186.6	2.626	0.001	2.626	0.001
32	1489.1	1489.6	2.660	0.001	2.66	0.001
31	1815.2	1814.8	2.670	0.001	2.67	0.001
30	2122.0	2122.6	2.721	0.001	2.721	0.001
29	2368.0	2368.6	2.451	0.001	2.451	0.001
28	2571.5	2572.1	2.740	0.001	2.740	0.001
27	2954.0	2954.6	2.662	0.001	2.662	0.001
26	3252.8	3253.4	2.613	0.001	2.613	0.001
25	3438.1	3438.7	2.832	0.001	2.832	0.001
24	3561.7	3562.4	2.861	0.001	2.861	0.001
23	3703.6	3704.3	2.781	0.001	2.781	0.001
22	3885.3	3886.0	2.271	0.001	2.271	0.001
21	4101.8	4102.5	2.281	0.001	2.281	0.001
20	4385.2	4385.9	2.371	0.001	2.371	0.001
19	4510.8	4511.6	2.368	0.002	2.368	0.002
18	4655.3	4656.1	2.481	0.001	2.481	0.001
17	4847.8	4848.7	2.286	0.003	2.286	0.004
16	5015.1	5016.3	2.169	0.002	2.169	0.004
15	5175.1	5176.6	2.462	0.003	2.462	0.003
14	5215.6	5217.2	2.758	0.004	2.758	0.004
13	5245.3	5246.9	2.792	0.006	2.792	0.006
12	5274.2	5275.9	2.855	0.005	2.856	0.005
11	5304.3	5306.0	2.716	0.020	2.715	0.010
10	5318.2	5320.0	2.754	0.006	2.755	0.007
9	5348.2	5350.0	2.722	0.020	2.721	0.010
8	5368.1	5370.0	2.667	0.008	2.667	0.008
7	5388.1	5390.0	2.653	0.007	2.654	0.007
6	5408.1	5410.0	2.653	0.007	2.653	0.007
5	5428.0	5430.0	2.713	0.008	2.712	0.008
4	5448.0	5450.0	2.688	0.005	2.688	0.005
3	5477.9	5480.0	2.704	0.005	2.704	0.005
2	5507.9	5510.0	2.716	0.005	2.715	0.005
1	5537.9	5540.1				

Table A-6. Apparent densities from 2018 Survey.

Station ID	Station TVD (ft)	Station WLD (ft)	Conventional Density (g/cm3)	Sigma Conv Density (g/cm3)	Inversion Density (g/cm3)	Sigma Inv Density (g/cm3)
37	23.56	23.56	2.138	0.001	2.142	0.001
36	229.96	230.02	2.321	0.001	2.320	0.001
35	661.58	661.64	2.435	0.002	2.436	0.002
34	851.60	851.76	2.513	0.001	2.513	0.001
33	1187.64	1187.87	2.624	0.001	2.624	0.001
32	1490.11	1490.58	2.658	0.001	2.658	0.001
31	1815.15	1815.79	2.669	0.001	2.670	0.001
30	2121.29	2122.00	2.720	0.001	2.719	0.001
29	2366.66	2367.38	2.452	0.001	2.452	0.001
28	2570.46	2571.18	2.740	0.000	2.740	0.000
27	2952.08	2952.88	2.662	0.000	2.662	0.000
26	3250.52	3251.06	2.612	0.001	2.613	0.001
25	3436.39	3436.95	2.831	0.001	2.830	0.001
24	3559.87	3560.44	2.865	0.002	2.863	0.002
23	3701.68	3702.03	2.781	0.001	2.782	0.002
22	3883.19	3883.53	2.271	0.001	2.272	0.001
21	4100.48	4100.83	2.282	0.001	2.282	0.001
20	4383.95	4384.34	2.376	0.001	2.377	0.001
19	4509.93	4510.34	2.372	0.001	2.373	0.001
18	4654.17	4654.63	2.482	0.001	2.482	0.001
17	4846.40	4846.96	2.288	0.001	2.288	0.001
16	5014.06	5014.83	2.173	0.001	2.174	0.001
15	5174.69	5176.02	2.468	0.002	2.473	0.002
14	5215.63	5217.02	2.749	0.003	2.744	0.003
13	5245.57	5247.02	2.785	0.004	2.786	0.003
12	5274.32	5276.00	2.847	0.005	2.842	0.004
11	5304.26	5305.99	2.693	0.014	2.687	0.006
10	5318.25	5320.01	2.761	0.007	2.768	0.004
9	5348.16	5349.99	2.726	0.009	2.710	0.006
8	5368.13	5370.00	2.628	0.009	2.640	0.006
7	5388.10	5390.01	2.625	0.008	2.631	0.005
6	5408.07	5410.02	2.672	0.008	2.671	0.005
5	5428.10	5430.04	2.687	0.008	2.682	0.005
4	5447.96	5449.99	2.696	0.005	2.697	0.004
3	5478.02	5480.03	2.695	0.006	2.695	0.004
2	5507.85	5510.00	2.693	0.005	2.689	0.004
1	5537.81	5540.00				

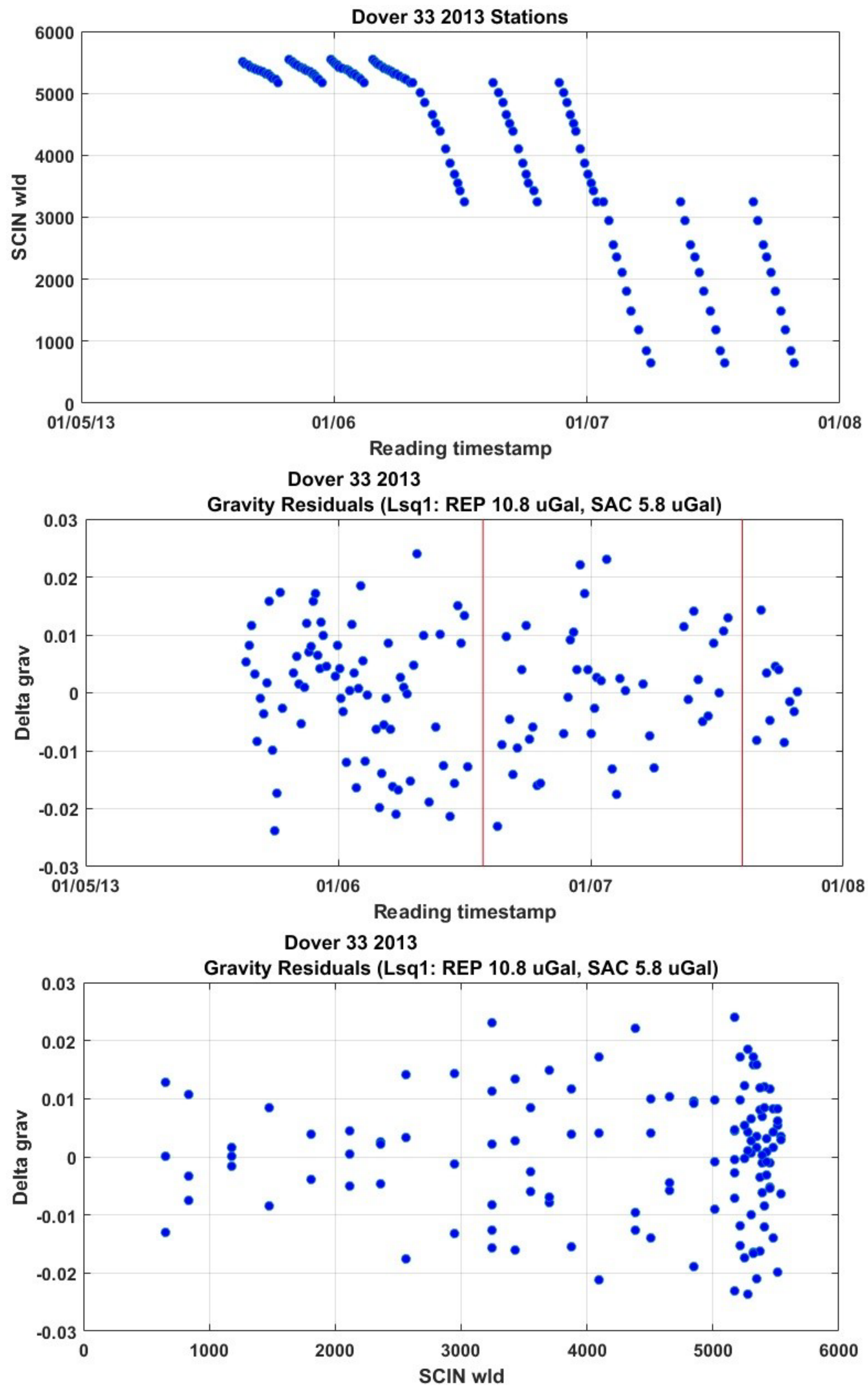

Figure A-1. 2013 survey stations (top) and gravity residuals versus time (middle) and depth (lower).

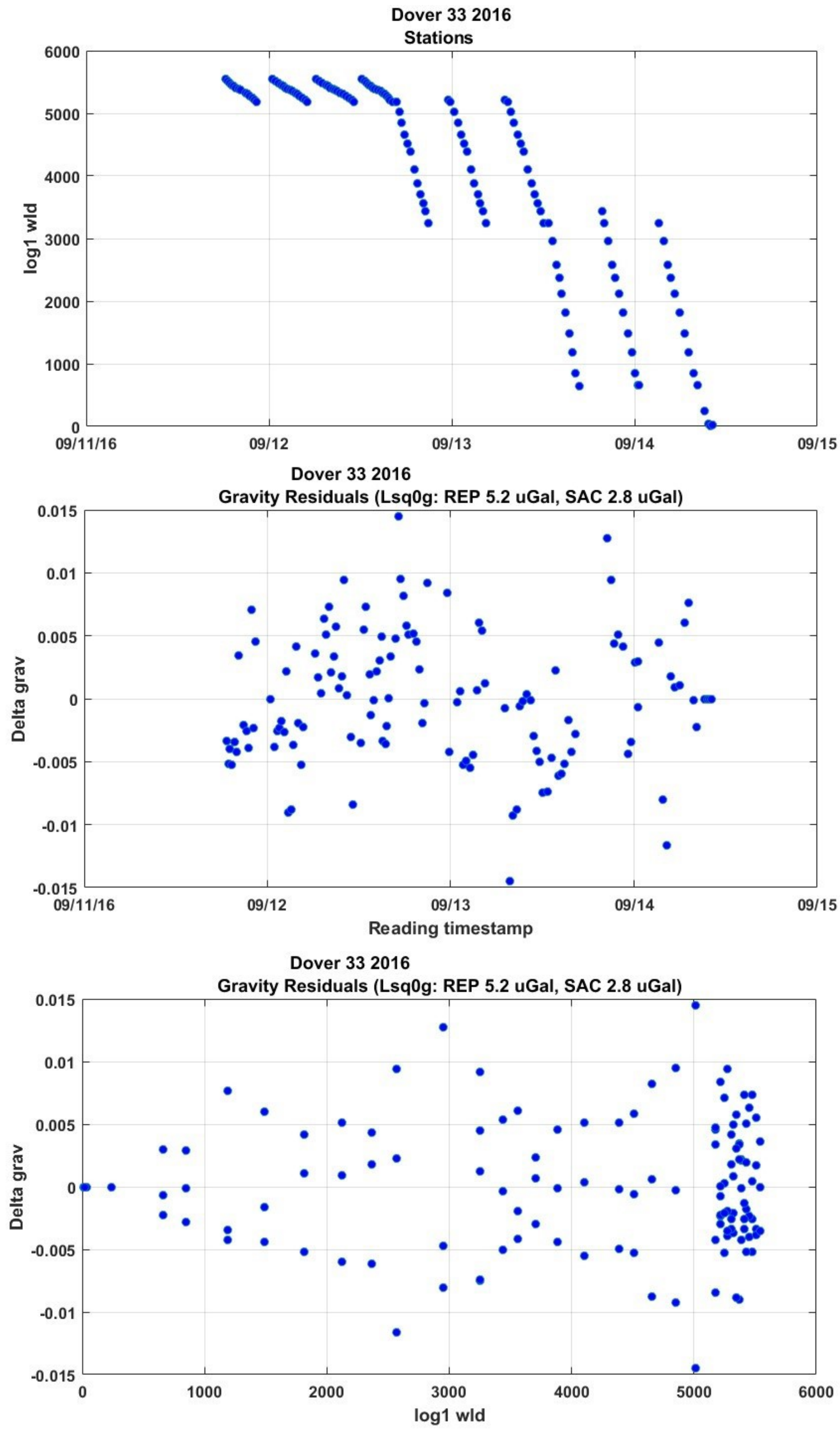

Figure A-2. 2016 survey stations (top) and gravity residuals versus time (middle) and depth (lower).

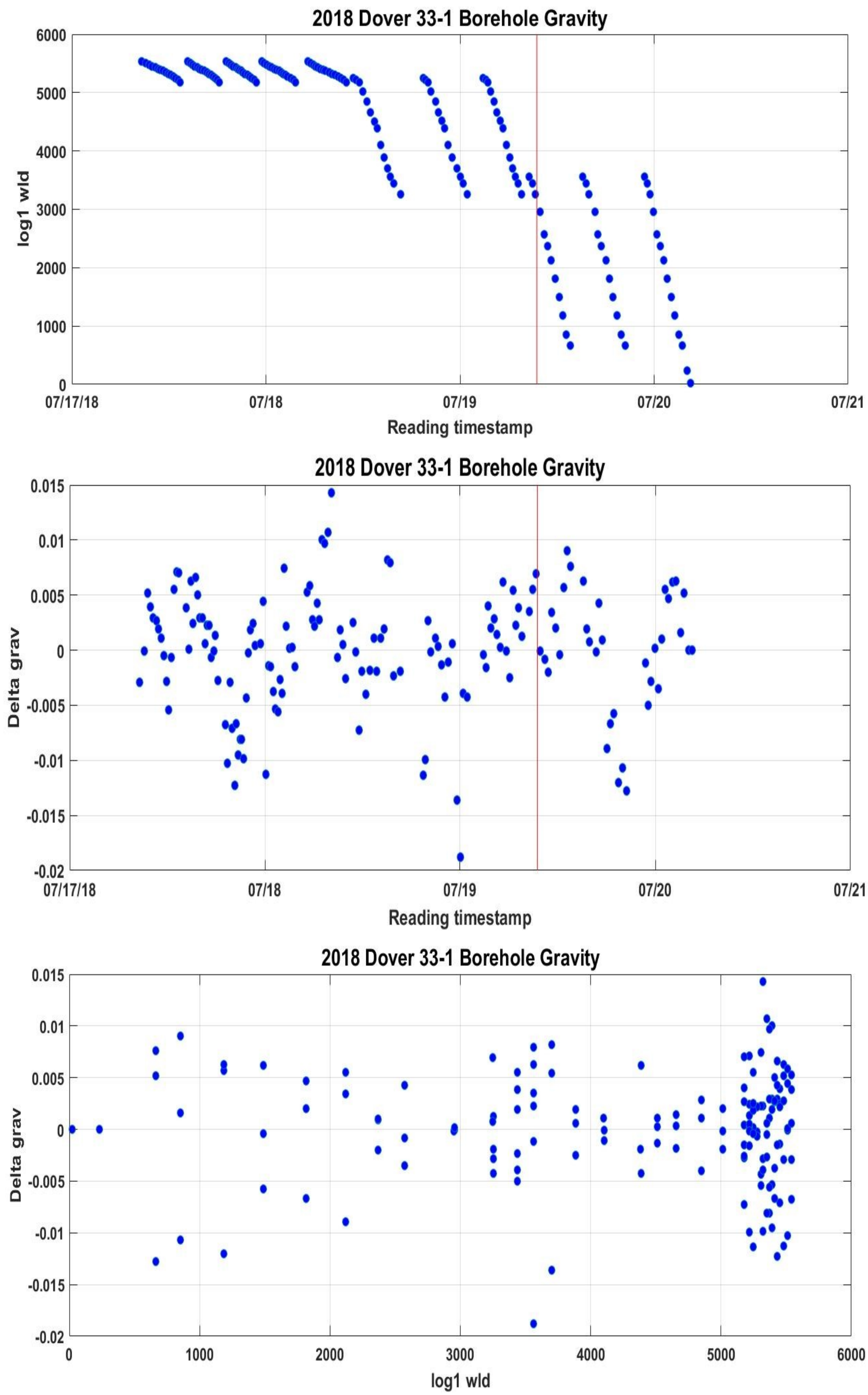

Figure A-3. 2018 survey stations (top) and gravity residuals versus time (middle) and depth (lower).